Kinetic and Mechanistic Studies of the I_2/O_3 Photochemistry

Juan Carlos Gómez Martín,* Peter Spietz, and John P. Burrows

Institute of Environmental Physics, University of Bremen, P. O. Box 330440, 28334 Bremen, Germany

Received: February 24, 2006; In Final Form: October 30, 2006

The atmospherically relevant chemistry generated by photolysis of I_2/O_3 mixtures has been studied at 298 K in the pressure range from 10 to 400 hPa by using a laboratory flash photolysis setup combining atomic resonance and molecular absorption spectroscopy. The temporal behaviors of I, I_2, IO, and OIO have been retrieved. Conventional kinetic methods and numerical modeling have been applied to investigate the IO self-reaction and the secondary chemistry. A pressure independent value of $k(\mathrm{IO} + \mathrm{IO}) = (7.6 \pm 1.1) \times 10^{-11}$ cm^3 molecule^{-1} s^{-1} has been determined. The pressure dependence of the branching ratios for the I + OIO and IOIO product channels in the IO + IO reaction have been determined and have values of 0.45 ± 0.10 and 0.44 ± 0.13 at 400 hPa, respectively. The branching ratios for the 2I + O_2 and I_2 + O_2 product channels are pressure independent with values of 0.09 ± 0.06 and 0.05 ± 0.03, respectively. The sensitivity analysis indicates that the isomer IOIO is more thermally stable than predicted by theoretical calculations. A reaction scheme comprising OIO polymerization steps has been shown to be consistent with the temporal behaviors recorded in this study. For simplicity, the rate coefficient has been asumed to be the same for each reaction $(\mathrm{OIO})_n + \mathrm{IO} \rightarrow (\mathrm{OIO})_{n+1}$, $n = 1, 2, 3, 4$. The lower limit obtained for this rate coefficient is $(1.2 \pm 0.3) \times 10^{-10}$ cm^3 molecule^{-1} s^{-1} at 400 hPa. Evidence for the participation of IO in the polymerization mechanism also has been found. The rate coefficient for IO attachment to OIO and to small polymers has been determined to be larger than $(5 \pm 2) \times 10^{-11}$ cm^3 molecule^{-1} s^{-1} at 400 hPa. These results provide supporting evidence for atmospheric particle formation induced by polymerization of iodine oxides.

Introduction

Iodine atoms are released in the troposphere by photolysis of molecular iodine[1−4] and a variety of volatile iodocarbons,[5,6] which are emitted in large part by the marine biosphere. Their atmospheric fate is primarily to react with O_3, forming the iodine monoxide (IO) radical:[7,8]

$$\mathrm{I} + \mathrm{O_3} \rightarrow \mathrm{IO} + \mathrm{O_2} \tag{1}$$

Reactions that convert IO back to iodine atoms without the formation of oxygen atoms can lead to a catalytic O_3 loss.[9] An example of this type of reactions is the disproportionation or self-reaction of IO, which has several channels:[10]

$$\mathrm{IO} + \mathrm{IO} \rightarrow \mathrm{I_2} + \mathrm{O_2} \quad \Delta H_r^0 = -170 \text{ kJ mol}^{-1} \tag{2a}$$

$$\rightarrow 2\mathrm{I} + \mathrm{O_2} \quad \Delta H_r^0 = -18 \text{ kJ mol}^{-1} \tag{2b}$$

$$\rightarrow \mathrm{I} + \mathrm{OIO} \quad \Delta H_r^0 = -48 \text{ kJ mol}^{-1} \tag{2c}$$

$$\xrightarrow{\mathrm{M}} \mathrm{I_2O_2} \quad \Delta H_r^0 = -108 \text{ kJ mol}^{-1} \tag{2d}$$

To determine the ozone destroying potential of iodine in the atmosphere, knowledge of the rate coefficient and branching ratios of reaction (2) and of the atmospheric fate of the iodine oxides OIO and I_2O_2 are required. Several studies have reported the value of the overall rate coefficient of reaction (2).[10] Iodine atoms are regenerated by channels (2b) and (2c). At daytime, the photolysis of I_2 followed by reactions (1), (2b), and (2c) produces a chain reaction destroying ozone. In general, the branching mechanism of reaction (2) is uncertain and not yet well established.[11−15]

The atmospheric fate of OIO[3,16,17] is currently under discussion.[18−22] Iodine condensable vapors are linked to new particle formation in the coastal marine boundary layer (MBL) at low tide and during the day.[23] Gas to particle conversion has been proposed as a potentially important sink for OIO. It is thought that iodine oxide particles can contribute significantly to the background aerosol and further grow into cloud condensation nuclei in the presence of additional condensable species.[24]

The photolysis of mixtures of ozone and different precursors of atomic iodine in laboratory studies[4,24−30] has demonstrated the occurrence of iodine-driven rapid particle production. Burkholder et al.[26] modeled the production of particles larger than 3 nm in a Teflon bag experiment by considering homogeneous nucleation of OIO. This mechanism comprises multiple OIO condensation−evaporation steps leading to a thermodynamically stable iodine oxide cluster on which particle growth starts:

$$(\mathrm{OIO})_n + \mathrm{OIO} \leftrightarrow (\mathrm{OIO})_{n+1} \tag{3}$$

Unfortunately, the experiments reported by Burkholder et al.[26] did not include the simultaneous measurement of gas-phase species.

Previous studies assume that the IO dimer represents the balance of the reaction products in the IO self-reaction at pressures higher than about 100 hPa.[13,29−32] However, this species has not been unequivocally assigned and its properties remain unknown. There is no information available about chemical sinks for I_2O_2. According to McFiggans et al.,[33] the

10.1021/jp061186c CCC: $37.00
Published on Web 12/14/2006

TABLE 1: Absorption Cross Sections of Iodine Species

species	λ (nm)	σ (10^{-17} cm^2 molecule^{-1})	fwhm (nm)[a]	ref
IO($v''=0$)	427.2 (4←0)	3.5 ± 0.3	0.12	32
IO($v''=1$)	449.3 (3←1)	4.5 ± 0.5	0.12	32
IO($v''>1$)	484.9 (1←2)	6.0 ± 0.5	0.12	32
OIO (0,0,0)	549.3 (5,1,0←0,0,0)	1.3 ± 0.3	0.35	32
I_2	500 (B←X continuum)	0.219 ± 0.002		40

[a] The measured OD versus time curves (fwhm = 1.3 nm) were converted to the resolution indicated in the table before scaling them to concentration.[39]

impact of the iodine chemistry on the tropospheric ozone and the aerosol enrichment on iodine depends critically on the fate of I_2O_2.

This paper presents a study of the gas-phase I_2/O_3 photochemistry by time-resolved absorption spectroscopy. The mixtures of I_2 and O_3 employed result in the formation of significant amounts of OIO and of higher iodine oxides. Although no specific measurements of particles have been performed, the formation of aerosol at longer reaction times has been observed. An important objective of the study is to gain a better understanding of the gas-phase chemistry of IO and OIO and the reactions producing higher oxides of iodine. In particular, the aims are: (a) to investigate the branching of the IO self-reaction at 298 K, and (b) to generate a plausible mechanism to explain the fates of OIO and I_2O_2.

Experimental Section

Apparatus. A sketch of the flash photolysis setup employed in these experiments can be found in a previous publication.[32] Iodine oxides were generated at 298 K in a 120 cm long and 5 cm diameter, temperature-stabilized quartz reaction vessel by flash photolysis of I_2/O_3 mixtures carried in a stable laminar flow of N_2 and/or O_2. A flow of I_2 in N_2 was produced by passing a stream of N_2 through a thermostated and pressure stabilized ($T = 273$ K) glass trap containing I_2. The mixtures could be diluted by an additional flow of pure N_2. O_3 was produced by passing a stream of O_2 through a silent discharge. The N_2 and O_2 (grade 4.8) were obtained from Messer−Griesheim and the I_2 (pro analysis grade) was obtained from from ACROS organics. The flows were controlled using calibrated mass flow controllers (MKS instruments). Calibrated capacitance barometers were employed to measure the pressure in the vessel (MKS instruments).

The photolysis flash system contains two Xenon flash tubes (Heimann). They emit a pulse of broadband radiation ranging from ultraviolet to visible and infrared. The electronics were such that a pulse having 0.1 ms full width at half-maximum (fwhm) resulted. The spectral distribution corresponds to the radiation of a black body at ~7000 K with some superimposed and broadened absorption lines. This radiation photodissociates I_2 as shown:[34−35]

$$I_2(X^1\Sigma_g^+) + h\nu \rightarrow I(^2P_{1/2}) + I(^2P_{3/2}) \quad (4a)$$

$$I_2(X^1\Sigma_g^+) + h\nu \rightarrow 2I(^2P_{3/2}) \quad (4b)$$

The extent of iodine photolysis determined in experiments in the absence of ozone was about 10%. The metastable iodine generated in channel (4a) is quenched as shown in eq 5:[35]

$$I(^2P_{1/2}) + O_2(X^3\Sigma_g^-) \rightarrow I(^2P_{3/2}) + O_2(a^1\Delta_g) \quad (5)$$

Such quenching takes less than 4 μs at 4 hPa of O_2. Optical filters between the tube and the vessel were used to limit the wavelength of the photolyzing radiation in the UV. Specifically, this enabled the elimination of the photolysis of O_3 in its Hartley and Huggins bands.[37] The upper limit for the extent of ozone photolysis determined experimentally (in the absence of I_2) was 0.05%.

After the photolysis of I_2, IO is formed via reaction (1) and OIO via reaction (2c). The time scale of the chemistry under study (typically being <30 ms for the mixing ratios of precursors considered, see Table 2) is short with respect to the purging time of the vessel (~3 s). This enabled the assumption of static mixture to be made for the analysis. The vessel was purged up to three times before each flash to remove secondary products, which might interfere in the reactions under study. For each experiment, 100 flashes were averaged.

The detection apparatus has been designed to simultaneously monitor all relevant molecular and atomic species.[32] Characteristic UV−vis molecular absorption of the light generated by a 150 W super-quiet Xe arc lamp (Hamamatsu) was measured along a White-type multipath optical arrangement (path length = 24.3 m). The light transmitted through the vessel was analyzed by using a 0.5 m Czerny−Turner spectrometer (Acton) operated with a 150 grooves mm^{-1} grating. A charge-coupled device (CCD) camera (Roper Scientific) with a 1024 × 1024 silicon detector chip (SiTE, 26 μm × 26 μm) was used to record spectra. The linear dispersion with this spectroscopic setup was 0.32 nm pixel^{-1}. This enabled the coverage of a spectral range of about 300 nm. The combination of the 150 grooves mm^{-1} grating with a slit width of 100 μm resulted in a spectral resolution of 1.3 nm fwhm.[32] Time series of spectra were obtained by operating the CCD camera in kinetic mode (80−160 μs effective time resolution). The detection limit is determined by the electronic noise of the CCD, the output of the analysis lamp, and the absorption of light by ozone. It varied between 0.01 units of optical density (OD) at 320 nm and 0.004 units at 500 nm. Thus, the minimum detectable concentrations for IO and OIO were 8×10^{10} molecule cm^{-3} and 2×10^{11} molecule cm^{-3}, respectively.

I_2 and O_3 concentrations were obtained either by measuring pure I_2 and O_3 spectra in static mode previous to the kinetic series and/or by using optical densities recorded in kinetic mode

TABLE 2: Experimental Conditions of Kinetic Datasets[a]

series[b]	N exp	P_{vessel} (hPa)	$[N_2]^c$ (10^{18})	$[O_2]^c$ (10^{18})	$[O_3]_0^d$ (10^{15})	$[I_2]_0^d$ (10^{13})	$[I]_{max}^e$ (10^{13})	$[IO]_{max}^f$ (10^{12})
1	7	40−400	0.6−10	0.4	2	5.4	1	7.5−8
2	6	100−400	0.6	2−10	2	5.4	1	6.5−7
3	8	40−400	0.6−10	0.4	0.7	4.4	1	5
4	11	10−40	0.1−0.6	0.1−0.4	0.5−2	2−6	3−9	2−8
5	6	10−40	0.1−0.6	0.1−0.4	0.5−2	0.3−1	2−6	1.5−5.5

[a] All concentrations are given in molecules or atoms cm^{-3} (see text). [b] N_2 and O_2 concentrations have been estimated from the total pressure in the vessel and the readout of the flow controllers. Uncertainty ~10%. [d] Uncertainty: <15% (see text). [e] Uncertainty: <14% (see text). [f] Uncertainty ~8% (see text).

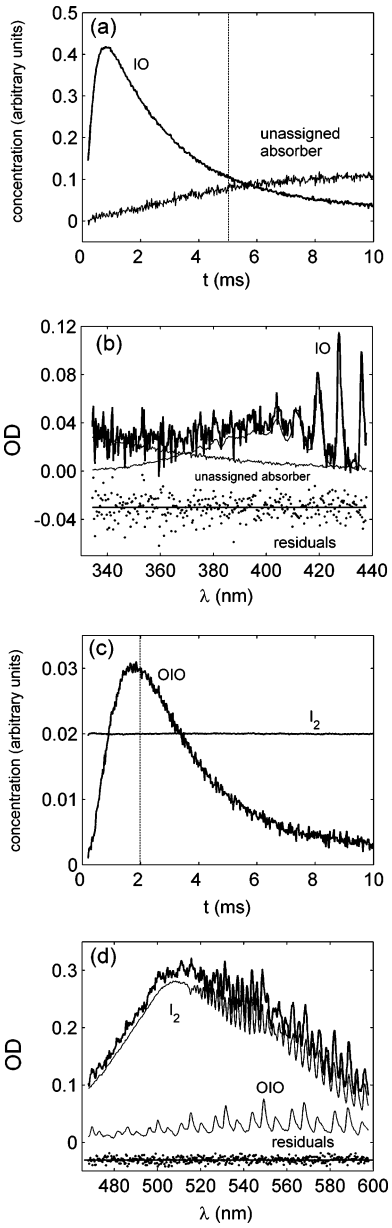

Figure 1. Example of separation of overlapping absorptions. Panel (a) shows the temporal behaviors (arbitrarily scaled) resulting from the spectral fitting of IO and an unassigned broadband absorber. Panel (c) shows the same for I_2 and OIO. The vertical dashed lines indicate the reaction times that correspond to the examples of spectral fits shown in panels (b) and (d). The thick lines are observed optical densities, the thin lines are scaled reference spectra, and the points are residuals. The residuals have been offset by −0.03 OD units for clarity.

after the photolysis flash. Error estimates (<15%) take into account random noise of the detection device as well as concentration drifts along the experiment and instability of the lamp and the optics. The temporal behavior of the OD versus time for each molecular absorption was retrieved from the time-resolved measurements of the CCD, following the deconvolution procedures explained by Gómez Martín et al.[32,38] Figure 1b shows a spectral fit corresponding to the separation of IO and an unassigned broadband absorber. Figure 1c shows an example of separation of I_2 and OIO. Instrumental effects on narrow spectral features (e.g., the maximum of the IO(4←0) band) caused by the coarse resolution were corrected by using the method described by Spietz et al.[39] The calibration of the OD temporal behaviors of molecules and radicals to concentration

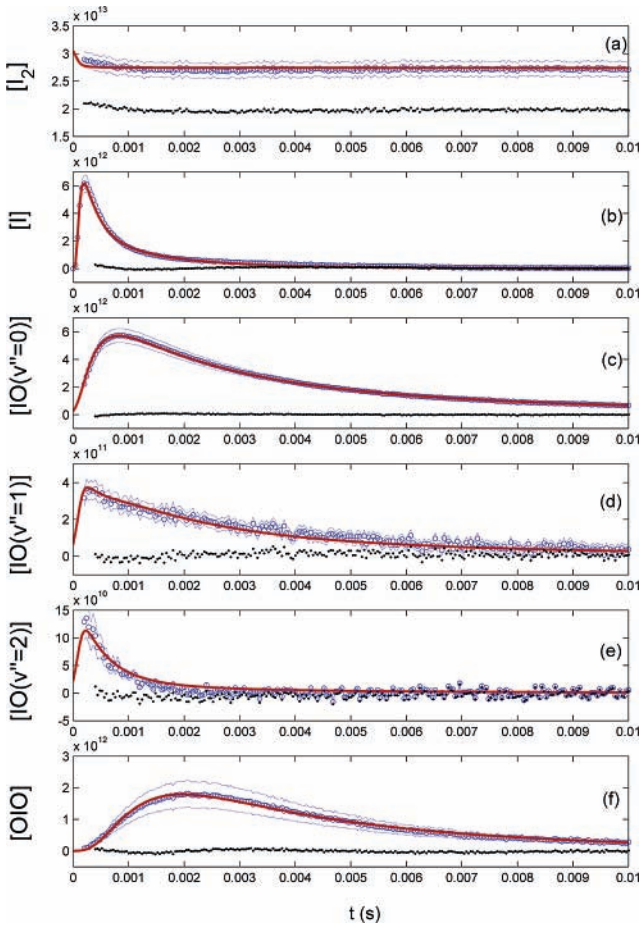

Figure 2. Group of concentration versus time curves (blue circles) measured in a typical experiment at 40 hPa. Concentrations are expressed in molecule cm^{-3}. Blue dashed lines indicate the error interval of the observations. The observational error arises mainly from uncertainties in the concentrations of the precursors and in the reference absorption cross sections used to scale the curves. The red curves are the results of an optimized simulation using the model contained in Table 3. The optimal parameters have been obtained by weighted nonlinear least-squares fitting. Residuals are given by black points.

was achieved by applying the Beer−Lambert law as follows:

$$[\mathrm{R}](t) = \frac{a_{\mathrm{R}}(\lambda_0,t)}{L\sigma_{\mathrm{R}}(\lambda_0)} \qquad \text{(i)}$$

where (t), $a_{\mathrm{R}}(\lambda_0,t)$, and $\sigma_{\mathrm{R}}(\lambda_0)$ are, respectively, the concentration versus time curve, the OD temporal behavior, and the absorption cross section at the wavelength λ_0 of the species R, and L is the path length. The vacuum wavelengths selected were: 427.2 nm for IO ($v'' = 0$), 459.3 nm for IO ($v'' = 1$), 484.9 nm for IO ($v'' = 2$), 500 nm for I_2, and 549.3 nm for OIO. The cross sections for these wavelengths are given in Table 1.[32,40] As a result of the application of techniques for reduction of noise and separation of overlapping absorptions,[38] the main source of uncertainty of the concentration versus time curves (Figure 2) is the uncertainty in the corresponding absorption cross section.[32] Concentration curves for higher iodine oxides also were obtained (e.g., Figure 1a). However, these data have not been used in the kinetic analysis because of their high uncertainty and ambiguous chemical assignment.

Iodine atoms were monitored by using atomic resonance absorption spectroscopy. $I(^2P_{3/2})$ resonance absorption of radiation, emitted by an electrodeless iodine lamp, was measured along a short path cross axis (0.055 m) of the reaction vessel

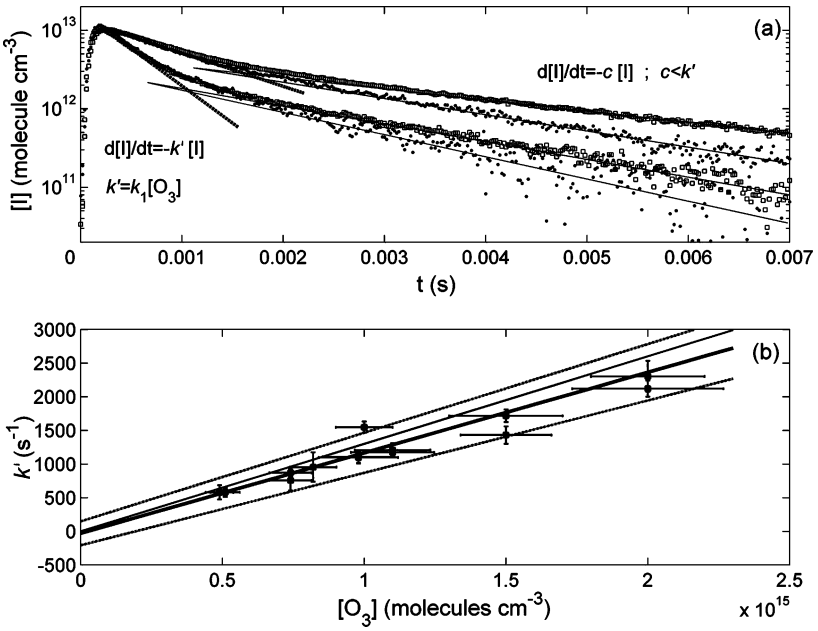

Figure 3. Panel (a) shows logarithmic plots of [I] as a function of time for 40 hPa (squares) and 400 hPa (points). The O_3 concentrations are 2×10^{15} molecule cm^{-3} (fastest decays) and 7×10^{15} molecule cm^{-3} (slowest decays). Panel (b) shows a plot of pseudo first-order decay coefficients k' versus [O_3] (see text). The correlation coefficient of the fit was $R^2 = 0.93467$. The slope of the thin solid line corresponds to the IUPAC recommendation. The dashed lines indicate the 95% confidence region.

by using a 0.25 m Czerny−Turner spectrometer with a 1200 grooves mm^{-1} holographic grating and a photomultiplier tube. The detection limit was approximately 10^{11} atoms cm^{-3}. Because of the large uncertainty of the oscillator strength of the 183.038 nm transition of I($^2P_{3/2}$),[41] the iodine atom curves have been empirically calibrated. To this end, experiments without ozone were undertaken in which $\Delta[I_2]$ and the corresponding increase of iodine atom resonance absorption were simultaneously measured. The change in the I($^2P_{3/2}$) absorbance was regressed against $2\Delta[I_2]$ to obtain a scaling factor. The regression curve was linear to a very good approximation for [I] $< 4 \times 10^{13}$ atoms cm^{-3} (the maximum [I] considered in kinetic experiments was 10^{13} atoms cm^{-3}). The combined uncertainty of the scaling factor and the raw data yielded a total estimated uncertainty at the maximum of the iodine atom concentration curves of ∼8%. This calibration has been checked by pseudo first-order fitting of the observed decays (Figure 3). Two linear sections can be observed in the log [I] curves. The slope k' of the first section (dashed line) is pressure independent and consistent with reaction (1). The rate coefficient $k_1 = (1.20 \pm 0.12) \times 10^{-12}$ cm^3 molecule^{-1} s^{-1} was obtained from the slopes of the first linear sections of the log [I] curves (Figure 3, panel b). This value is in good agreement with the IUPAC recommendation for reaction (1) at 298 K within the error limits.[10]

The curvature and the second linear section result from iodine atom recycling by reaction (2). The uncertainty of this sections is larger, as a result of a potential inhomogeneous distribution of iodine atoms along the reaction vessel resulting from screening of the flash by the joints of the cross axis of the reaction vessel (see Figure 1 in Gomez Martín et al.[32]). This would have a nonlinear impact on that part of the [I] curves, which depend on [IO]^2. To quantify this effect, an independent calibration of the iodine atom curves has been carried out using the oscillator strength determined by Spietz et al.[41] The difference between the iodine concentration obtained by both calibration methods results from the combination of the uncertainty in the oscillator strength and inhomogeneous distribution of iodine atoms. A series of kinetics simulations have been performed for the range of conditions considered in this work, assuming a worst case scenario in which the whole difference results from inhomogeneous distribution. For the largest iodine atom yield from reaction (2) reported in the literature,[11] this effect has been found to be ∼6% at the point where the peak IO concentration is reached. This additional systematic error must be taken into account in the calculation of k_2.

Experiments. Three analogous series of experiments were carried out over a range of pressures between 40 and 400 hPa (see Table 2). Two series were conducted with N_2 and one with O_2 as the diluting gas. On each serie, the initial amounts of I_2 and O_3 in the vessel were kept constant, while the pressure was varied by increasing the flow of the diluting gas. Constancy of $[I_2]_0$ and $[O_3]_0$ at different pressures was verified to be generally better than 10%. No attempt was made to search for optimal mixtures appropriate for simple kinetic modeling of the IO temporal behavior. Rather, in the first series of experiments the concentrations of precursors were set to maximize the amount of radicals produced. The second series was run to check a potential influence of the third body on the chemistry under study. The third series was intended to check possible dependencies on the initial [O_3].

In addition, two further series of experiments were conducted at lower pressures (10−40 hPa). In this case the pressure was changed by varying the aperture of the valve in the exhaust of the vessel. Thus, the initial concentrations of the precursors changed within the series, although their relative concentration was kept constant. Series 5 was run to investigate the potential effect of varying the initial I_2 concentration. Experimental conditions of the 38 datasets analyzed are summarized in Table 2. Additionally, experiments without O_3 were carried out before each series in order to determine the photolysis rate of I_2.

The length of each experiment was defined by time required for the consumption of OIO. The exposure time of the CCD was set accordingly to register the major part of the OIO in the data recordings. For series 1 to 3 the duration of the experiments was about 10 ms, and the exposure time was adapted to obtain data recordings of this duration. For series 4 and 5 the duration

TABLE 3. Chemical Mechanism Used for the Investigation of the I_2/O_3 Photochemical System

reaction	rate coefficient	ref
$I_2 + h\nu \rightarrow I(^2P_{1/2}) + I(^2P_{3/2})$	$\sim 300\ s^{-1}$	[a]
$I_2 + h\nu \rightarrow 2I(^2P_{3/2})$	$\sim 800\ s^{-1}$	[a]
$I(^2P_{1/2}) + O_2 \rightarrow I(^2P_{3/2}) + O_2(a^1\Delta_g)$	$2.6 \times 10^{-11}\ cm^3\ molecule^{-1}\ s^{-1}$	36
$IO + h\nu \rightarrow I + O(^3P)$	$\sim 2400\ s^{-1}$	[a]
$IO + h\nu \rightarrow IO(v''=1)$	[b]	
$IO + h \rightarrow IO(v''=2)$		
$IO(v'') + M \rightarrow IO(v''-1) + M;\ v''=1,2,\Sigma$ [c]	$2.2 \times 10^{-15}\ cm^3\ molecule^{-1}\ s^{-1}$	this work
$IO(v''-1) + M \rightarrow IO(v'') + M;\ v''=1,2,\Sigma$	$\varphi \times 2.2 \times 10^{-15}\ cm^3\ molecule^{-1}\ s^{-1}$ [d]	
$O_3 + O_2(a^1\Delta_g) \rightarrow 2O_2 + O(^3P)$	$3.8 \times 10^{-15}\ cm^3\ molecule^{-1}\ s^{-1}$	64
$O_2 + O + M \rightarrow O_3 + M$	$5.9 \times 10^{-24}\ cm^6\ molecule^{-2}\ s^{-1}$	64
$I_2 + O \rightarrow IO + I$	$1.4 \times 10^{-10}\ cm^3\ molecule^{-1}\ s^{-1}$	10
$IO + O \rightarrow O_2 + I$	$1.4 \times 10^{-10}\ cm^3\ molecule^{-1}s^{-1}$	10
$I + O_3 \rightarrow IO + O_2$	$1.3 \times 10^{-12}\ cm^3\ molecule^{-1}\ s^{-1}$	10
$IO + IO \rightarrow I_2 + O_2$	Fitted k_{2a}	
$IO + IO \rightarrow 2I + OIO$	Fitted k_{2b}	
$IO + IO \rightarrow I + OIO$	Fitted k_{2c}	
$IO + IO \rightarrow I_2O_2$	Fitted k_{2d}	
$(OIO)_n + OIO \rightarrow (OIO)_{n+1};\ n = 1, 2, 3, 4$	Fitted k_{OIO+R}	
$(OIO)_n + IO \rightarrow (OIO)_n IO;$ $n = 1,2,3,4$	Fitted k_{IO+R}	
$(OIO)_n(IO)_m + IO \rightarrow (OIO)_n(IO)_{m+1}$ n=1,2,3,4; m = 1,2	k_{IO+R}	
$(OIO)_n(IO)_m + OIO \rightarrow (OIO)_{n+1}(IO)_m$ n = 1,2,3,4; m = 1,2	k_{OIO+R}	
$(IO)_n + IO \rightarrow (IO)_{n+1};\ n = 1, 2, 3, 4$	k_{IO+R}	
$(IO)_n + OIO \rightarrow (IO)_{n+1}IO;\ n = 1, 2, 3, 4$	k_{OIO+R}	

[a] The photolysis rate refers to the maximum of the flash photolysis pulse ($t \sim 90\ \mu s$). [b] Estimated for each experiment by fitting simplified model to reduced datasets. May include both photolytic and chemical sources associated to excited-state chemistry. [c] Σ represents the rest of vibrational excited estates of IO considered as a single species. [d] Thermal activation rates (inverse reaction (6)) can be derived as a product of the deactivation rates k_6 and the ratio of the corresponding Boltzmann factors of the IO oscillator. $\varphi = f_B(v''+1)/f_B(v'')$ indicates the ratio of Boltzmann factors for vibrational quantum numbers $v''+1$ and v''.

of the experiments changed between 10 and 30 ms and the length of the data recordings is 20ms.

Data Analysis

In Figure 2, a group of curves measured in a typical experiment at 40 hPa is shown. Although the complexity of I_2/O_3 photochemistry is recognized, classical kinetic analyses of these concentration versus time curves have been carried out to gain insight into the chemical mechanism. A second analysis of the same data has been performed by numerical integration of the system of ordinary differential equations (ODE) arising from the complex model developed to describe the chemical system. This chemical model is shown in Table 3. A numerical integration algorithm based on the numericaldifferentiation formulas[42] has been employed to solve this stiff ODE system. As a result of the finite duration of the photolysis pulse, the photolysis rates of I_2 are time dependent, and therefore a parametrization of the flash temporal behavior must be included in the simulations. In addition, a moving average smoothing of the simulated intensity versus time curves is required to model the finite (4−5 pixel wide) temporal characteristic function of the CCD chip.[31,32,43] After simulation and smoothing, the relevant simulated curves are concatenated in a single vector, which is fitted to the analogous vector of observations. A constrained weighted least-squares algorithm has been used to find the optimal parameters.[44] The weight of each concentration curve in the fit is inversely proportional to its uncertainty.

Results

(a) Conventional Kinetic Analysis. *Rate Coefficient and Branching Ratios of Reaction of the IO Self-Reaction.* The curvature of $[IO]^{-1}$ indicates that IO does not decay in a simple second-order manner. Rather, a loss in addition to reaction (2) and a production of IO are identified as being active during the decay (Figure 4). In general, the IO decays are well described by combining a first and a second-order loss processes. However, the minima of the least-squares cost function are not well defined for the two free parameters considered, and in addition the source of IO cannot be accounted for. These fits yield pseudo first-order rate coefficients for the secondary loss of about 100 s^{-1}. To avoid these uncertainties and estimate the rate coefficients, a steady state analysis of the maxima of the [IO] versus time curve (Figure 2c) has been carried out by

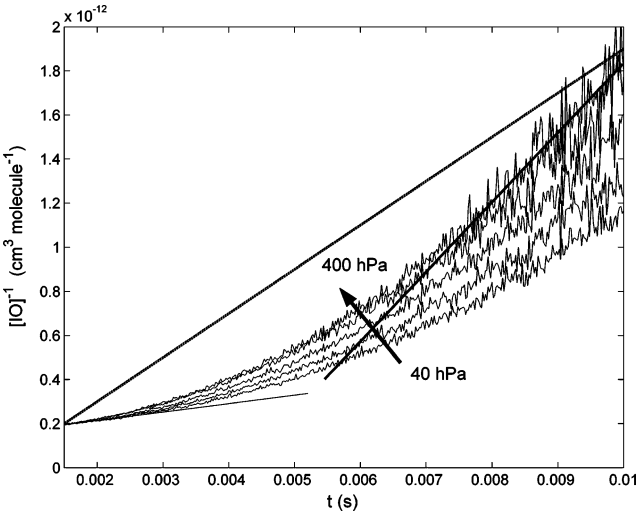

Figure 4. Plots of $[IO]^{-1}$ as a function of time for different pressures, showing nonsecond-order behavior of IO. The dashed line indicates the linear behavior expected for $[IO]^{-1}$ when IO decays in second order (rate coefficient recommended by the IUPAC[10]). The recycling of iodine atoms through the IO self-reaction and subsequent IO reformation are responsible for the smaller slope in the initial steps (thin solid line). In the final steps, further sinks of IO cause an increase of the slope (thick solid line) with respect to the second-order rate coefficient.

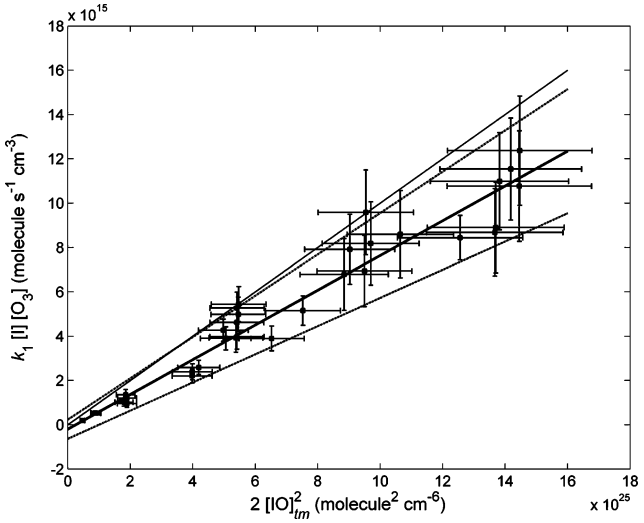

Figure 5. Steady state analysis of the [IO] versus time curves. An estimation of k_2 has been obtained by linear regression with error in both coordinates (thick line). The slope of the thin solid line corresponds to the IUPAC recommendation. The correlation coefficient of the fit was $R^2 = 0.94116$. The dashed lines indicate the 95% confidence region.

considering reactions (1) and (2). At the maximum of [IO] (reaction time t_m), the rate of change of IO concentration is zero as shown in eq (ii):

$$0 = \left.\frac{d[\mathrm{IO}]}{dt}\right|_{t_m} = k_1[\mathrm{O_3}]_{t_m}[\mathrm{I}]_{t_m} - 2k_2[\mathrm{IO}]_{t_m}^{\ 2} \Rightarrow$$

$$k_1[\mathrm{O_3}]_{t_m}[\mathrm{I}]_{t_m} = 2k_2[\mathrm{IO}]_{t_m}^{\ 2} \quad \text{(ii)}$$

A plot of the rate of production of IO, $k_1[O_3]_{t_m}[I]_{t_m}$, by reaction (1) versus $[IO]_{t_m}^2$ is shown in Figure 5. The k_2 is determined from the slope of the plot of $k_1[O_3]_{t_m}[I]_{t_m}$ as a function of $[IO]_{t_m}^2$ and estimated by a least-squares fitting procedure taking experimental error in both coordinates into account.[45] The error in the knowledge of the dependent variable $k_1[O_3]_{t_m}[I]_{t_m}$ comprises of the errors in $[O_3]$ (~11%) and [I] (~14%), and the knowledge of the rate coefficient k_1, which has a literature value $k_1 = (1.3 \pm 0.05) \times 10^{-12}$ cm^3 molecule^{-1} s^{-1},[10] while that of the independent variable includes an 8% uncertainty in the IO absorption cross section.[32] The rate coefficient obtained for reaction (2) in this manner is $k_2 = (7.8 \pm 1.2) \times 10^{-11}$ cm^3 molecule^{-1} s^{-1} with the error interval given being the at 95% confidence level. No pressure dependence can be discerned outside the 95% confidence region by fitting separately the data obtained at low and high pressures.

In Figure 3a, two separate linear regions in the plot of log [I] versus time are identified. The slowing down of the loss rate provides evidence for a source of [I]. The temporal behavior of this part of the decay of I atoms combines loss through reaction (1) and production via (2b) and (2c). The slopes of these regions of the logarithmic plots of [I] versus time are shown in Figure 3 and are pressure dependent. This implies that reactions (2b) and (2c) are pressure dependent. Assuming that the only processes relevant for iodine atoms are reactions (1), (2b), and (2c), the rate coefficient of the sum of iodine producing channels $k_{2b} + 0.5k_{2c}$ can be estimated by regression as follows:

$$-c[\mathrm{I}] = \frac{\mathrm{d}[\mathrm{I}]}{\mathrm{d}t} = -k'[\mathrm{I}] + 2(k_{2b} + 0.5k_{2c})[\mathrm{IO}]^2 \Rightarrow$$

$$(k' - c)[\mathrm{I}] = 2(k_{2b} + 0.5k_{2c})[\mathrm{IO}]^2 \quad \text{(iii)}$$

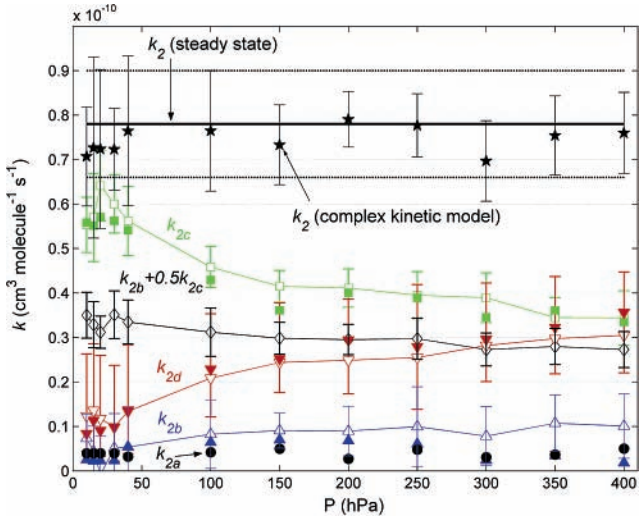

Figure 6. Overall rate coefficient (solid thick line) with its corresponding uncertainty (thin dotted line), rate coefficient of iodine atom producing channels (diamonds), and rate coefficients of individual channels of reaction (2) (circles, channel (2a); triangles up, channel (2b); squares, channel (2c); triangles down, channel (2d)). Open symbols connected by a thin line correspond to conventional kinetic analysis and filled symbols to optimized simulations. For clarity, only the uncertainties of the conventional kinetic analysis for the different channels are shown. Five pointed stars with error bars indicate the values of k_2 obtained by adding the rate coefficients of the individual channels obtained from optimized simulations.

where $k' = k_1[O_3]$ and c are the observed slopes of the log [I] curve (see Figure 3a). The values of $k_{2b} + 0.5k_{2c}$ obtained with this method are pressure dependent and decrease by about 20% from 10 hPa to 400 hPa (Figure 6).

Direct experimental evidence for the channel (2c) was obtained by Himmelmann et al.[46] in our laboratory with the first observation of OIO in the gas phase. To investigate the order of the rate of loss of OIO, plots of log [OIO] and $[OIO]^{-1}$ versus time were made and are shown in Figure 7. The decay of OIO in time is much closer to first order than second order. This implies that the disproportionation, or self-reaction, of OIO alone cannot explain the decay of OIO in the system. A regression analysis of the [OIO] versus time curve utilizing the cumulative integral of $[IO]^2$ and [OIO] has been undertaken to obtain estimates of the rate coefficient of reaction (2c) and the effective pseudo first-order loss rate coefficient for OIO:

$$[\mathrm{OIO}](t) - [\mathrm{OIO}]_0 =$$

$$k_{2c}\int_0^t ([\mathrm{IO}](t))^2\mathrm{d}t - k'_{\mathrm{OIO}\rightarrow\mathrm{loss}}\int_0^t [\mathrm{OIO}](t)\mathrm{d}t \quad \text{(iv)}$$

As shown in Figure 6, the results of the analysis indicate that k_{2c} is pressure dependent. The values of k_{2b} can be determined by combining the results obtained for $k_{2b} + 0.5k_{2c}$ and k_{2c}. Channel (2b) appears to be of minor importance in the IO self-reaction under the conditions studied.

Fate of OIO in the System. The pseudo first-order decay rate coefficient $k'_{\mathrm{OIO}\rightarrow\mathrm{loss}}$ has a small pressure dependence between 40 and 400 hPa (Figure 8a) and takes values around 800 s^{-1}. If a single bimolecular reaction were responsible for the removal of OIO, assuming a collision rate of 2×10^{-10} cm^3 molecule^{-1} s^{-1} as the upper limit for the rate constant, then the reaction partner is required to have a concentration larger than about 4×10^{12} molecule cm^{-3} and to persist for at least 10 ms after the photolysis flash. Of the reactants and products excluding O_2 and N_2, only I_2 and O_3 fulfill these conditions (see Figure 2 and Table 2).

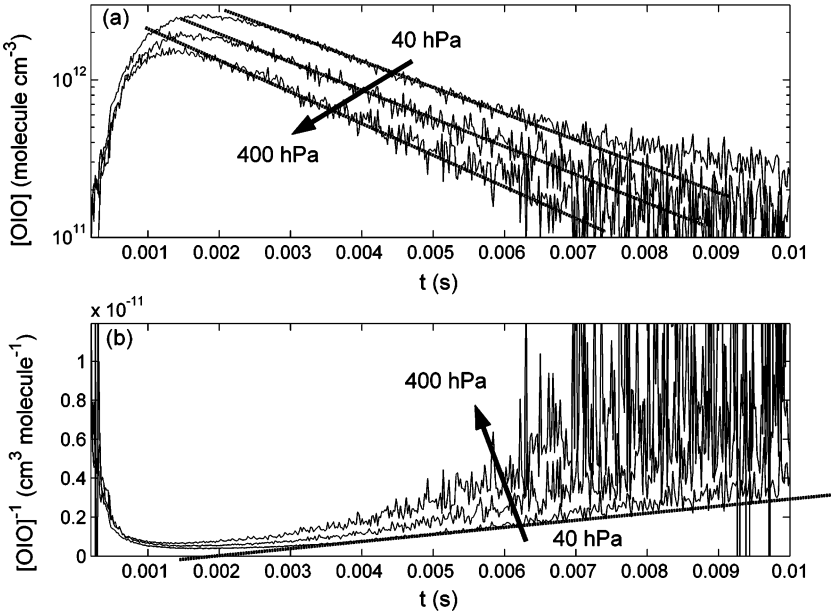

Figure 7. Plots of [OIO](*t*) in logarithmic scale (panel (a)) and [OIO]$^{-1}$(*t*) (panel (b)). The temporal behavior of OIO is more consistent with pseudo first order. As shown in panel (b), the OIO self-reaction does not explain the decay of OIO.

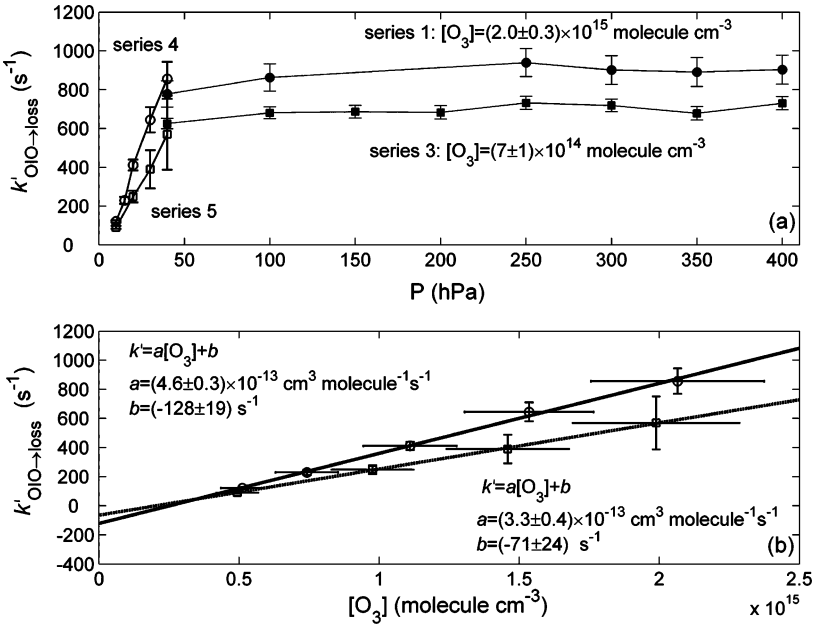

Figure 8. Panel (a) shows the apparent pseudo first-order decay rate coefficient (in s^{-1}) of OIO obtained from equation (iv). Individual results for four series of measurements are shown (filled circles, series 1; filled squares, series 3; empty circles, series 4; empty squares, series 5). Series 1 and 3 were run with a 3-fold difference in $[O_3]_0$. Panel (b) shows linear fits of $k'_{OIO\rightarrow loss}$ against O_3 for series 4 (circles, solid line) and 5 (squares, dashed line). A 6-fold drop of $[I_2]$ (series 5) caused a 40% decrease of the slope.

A direct proportionality between $k'_{OIO\rightarrow loss}$ and $[O_3]$ is not observed. The 3-fold change in $[O_3]_0$ does not result in a 3-fold smaller value for $k'_{OIO\rightarrow loss}$ (see Figure 8, series of experiments 1 and 3), and therefore the reaction with O_3 is discounted as the explanation of the pseudo first-order behavior of OIO. The decrease of $k'_{OIO\rightarrow loss}$ for $P < 40$ hPa cannot be directly interpreted as a pressure dependence, because the concentration of the precursors in the experiments recorded at these pressures also varied. Figure 8b shows linear fits of $k'_{OIO\rightarrow loss}$ against $[O_3]_0$ for experimental sets 4 and 5. In both cases, the intercepts are significantly different from zero, indicating again that $k'_{OIO\rightarrow loss}$ is not directly proportional to $[O_3]_0$.

A 6-fold decrease of $[I_2]_0$ causes a significant but not proportional decrease of $k'_{OIO\rightarrow loss}$ (Figure 8b). It is assumed that I_2 does not react with OIO, and the observed decay of OIO is therefore attributed to be dependent on the concentrations of iodine oxides generated at higher I atom concentrations.

Production and Loss of Excited IO Species. In the experiments performed at pressures lower than 100 hPa, vibrational bands of IO corresponding to transitions $v' \leftarrow v''$ with v'' up to 7 have been observed.[47] Figures 2d and 2e show, respectively, the temporal behaviors of the concentrations of IO ($X^2\Pi_{3/2}$, $v'' = 1$) and IO ($X^2\Pi_{3/2}$, $v'' = 2$), recorded at 40 hPa. The temporal behaviors of the three IO species observed are clearly different. The peak concentrations of vibrationally excited IO occur immediately after the flash, and relaxation to thermal equilibrium takes about 3 ms. After thermal equilibrium is established at 298 K, the observed optical densities corresponding to transitions from levels $v'' > 1$ are below the detection limit and the ratio of IO ($X^2\Pi_{3/2}$, $v'' = 1$) to IO ($X^2\Pi_{3/2}$, $v'' = 0$) is constant and

about 0.05 (see Figure 9). Assuming a Boltzmann distribution of the IO population, the ratio calculated using the vibrational constants reported by Bekooy et al.[48] is ~0.04. As the pressure is increased, the peak concentration of IO($X^2\Pi_{3/2}$, $v'' > 0$) decreases and thermal equilibrium is more rapidly achieved. For pressures above 100 hPa, the thermal equilibrium is achieved within the first time step of the experiment.

The source of the nonequilibrium population is attributed to processes, which occur during the flash, including reaction (1). The most important sink for IO($X^2\Pi_{3/2}$, $v'' > 0$) is collisional quenching and is shown as:

$$\mathrm{IO}(X^2\Pi_{3/2}, v'' > 0) + \mathrm{M} \rightarrow \mathrm{IO}(X^2\Pi_{3/2}, v''\text{-}1) + \mathrm{M} \quad (6)$$

The observed exponential decays of IO($X^2\Pi_{3/2}$, $v'' = 2$) (Figure 2e) are consistent with reaction (6). Assuming that collisional quenching is the dominating process, the rate coefficient of reaction (6) with $v'' = 2$ can be estimated by the regression analysis of the time constants of the observed decays and [M]. As a result, $k_{6,v''=2}$ is estimated to be $(2.2 \pm 0.5) \times 10^{-15}$ cm^3 molecule^{-1} s^{-1}. The nonzero intercept of the regression, which could be indicative of de-excitation by emission, is statistically not significant. The value obtained for k_6 is a lower limit because relaxation of IO ($v'' = 3$) to IO ($v'' = 2$) has been neglected.

At the lowest pressures, the concentrations of vibrationally excited IO are sufficiently large that their collisional quenching contributes to the rate of production of IO ($v'' = 0$). For these experiments, chemical removal of the nonequilibrium concentration of vibrationally excited IO, e.g., by reaction with IO ($v'' = 0$), cannot be ruled out. Although the amount of IO ($X^2\Pi_{3/2}$, $v'' = 2$) does not show a strong anticorrelation with [IO ($v'' = 0$)], it was not possible to separate the contribution of physical quenching of IO ($v'' = 2$) from that of potential chemical removal processes.

(b) Complex Kinetic Modeling. *Proposed Mechanism.* The conventional kinetic analysis described in the preceding section illustrates the complexity of the I_2/O_3 photochemical system. Many of the reactions are poorly characterized or even unknown, e.g., the dissociation of the IO dimer and the consumption of OIO. To investigate the mechanism, simulations of the chemical constituents derived from chemically plausible reaction schemes have been mathematically compared with the observations. In this manner, a mechanism able to reproduce the experimental data, whose reaction steps are listed in Table 3, was identified.

Ground state iodine atoms are generated in reactions (4)−(5). In the presence of an excess of ozone, sinks for iodine atoms other than reaction (1) have been judged to be unimportant. In addition, no enhanced I_2 reformation has been observed, which could indicate a molecule complex mechanism[15,49] resulting in an enhanced I-atom recombination. The major source of IO in the system is reaction (1). Reaction (2) is the primary sink for IO. At the lowest pressures under study, the initial amount of vibrationally excited IO is comparable to ground state IO (Figure 9). Therefore, activation and deactivation of IO vibrational states have been considered. It has been assumed that the quenching of all vibrational states proceeds at the same rate ($k_{6,v''=2}$). A small fraction of ozone (<0.05%) could be photolyzed. Some photolysis of newly formed IO may also occur as a result of the relatively long pulse of photolytic radiation. Ozone would by subsequently regenerated by combination of O(^{3}P) with O_2 and IO would be formed by reaction of O(^{3}P) with I_2. As a result of the large excess of I_2 over O(^{3}P), this minor source of IO has only an influence on the value of [IO] in the initial time step of the data recordings. It is essentially impossible to distinguish between both sources of O(^{3}P). For the conditions of this study, O_3 photolysis can be assumed to be insignificant.

The information provided by conventional kinetic analysis of the OIO build up and decay and the mechanism proposed in previous studies,[24−27] indicate that the following series of reactions appears to describe the OIO behavior well:

$$(\mathrm{OIO})_n + \mathrm{OIO} \rightarrow (\mathrm{OIO})_{n+1} \quad n = 1,2,... \quad (7)$$

where $(OIO)_n$ are polymeric structures.[24] The use of a common rate coefficient for all reactions encompassed in reaction (7)[49] has been preferred to individual fixed collision rates derived from kinetic theory to avoid the uncertainties in the size and density of these molecules. This recognizes that one of the steps is rate limiting. The rather simplistic assumption of a common value of k_7 is supported by the following arguments:

(a) Independently of the density assumed for the $(OIO)_n$ clusters (assuming spherical geometry), the differences between the collision frequency factors for $n = 1,..,4$ are small.

(b) The high dipole moment of OIO[27] suggests that the rate coefficients could be dominated by long-range interaction rather than the collision frequency.

The set of reactions (7) reproduces reasonably the observed OIO decay with $n_{max} \geq 4$. However, the common rate coefficient for reactions (7) obtained in these preliminary fits is larger than the collision frequency factors by a factor of 2−3. In addition, a late sink for IO is missing (see Figure 4). The rather large pseudo first-order rate coefficients estimated for this loss process by simple kinetic analysis ($k' \sim 100$ s^{-1}, see previous section) indicate that the reaction of IO and O_3 cannot be responsible for such sink.[26,50] These facts have suggested the attachment of IO and OIO units to form the complex polymeric adducts:

$$(\mathrm{OIO})_n + \mathrm{IO} \rightarrow (\mathrm{OIO})_n\mathrm{IO} \quad n = 1, 2,... \quad (8)$$

$$(\mathrm{OIO})_n(\mathrm{IO})_m + \mathrm{IO} \rightarrow (\mathrm{OIO})_n(\mathrm{IO})_{m+1} \quad n = 1, 2,...; m = 1,2,... \quad (9)$$

$$(\mathrm{OIO})_n(\mathrm{IO})_m + \mathrm{OIO} \rightarrow (\mathrm{OIO})_{n+1}(\mathrm{IO})_m \quad n = 1, 2,...; m = 1,2,... \quad (10)$$

A common rate coefficient (k_{IO+R}) has been assigned to all reactions consisting of the attachment of IO to oligomers (reactions (8) and (9)) and another (k_{OIO+R}) for the attachment of OIO (reactions (7) and (10)). This assumption builds on our knowledge of the different dipole moments of IO and OIO.[28] The inclusion of these reactions enables us to reproduce all experimental curves, and values for the reaction coefficients near the collision rates are calculated. It has been observed that the values $n_{max} = 4$ and $m_{max} = 2$ are enough to reproduce the data on the time scale of our experiments, and that by increasing this value, no further improvement in the correlation coefficient or significant changes in the optimal values for the rate constants is obtained. The rate coefficient of the reaction IO + OIO (8, $n = 1$) was considered initially as an independent free parameter, but the results obtained were essentially equal to those obtained for k_{IO+R} and the quality of the fits was not improved. In addition, the error estimates for k_{IO+R} and k_{OIO+R} were larger, thus indicating a redundancy between k_{IO+R} and k_{IO+OIO}. On the other hand, the inclusion of IO + OIO in the group of reactions (10) ($n = 0$, $m = 1$) resulted in smaller values of k_{OIO+R} and negligible values of k_{IO+R} with poor reproduction of the experimental OIO concentration curve and larger values of the χ^2 cost function in the multiparameter-fitting algorithm.

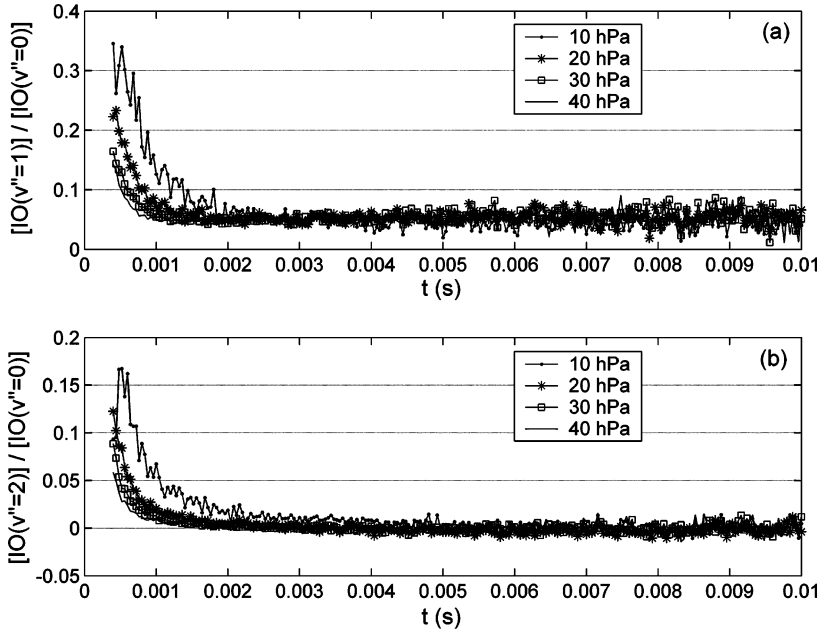

Figure 9. Ratios [IO ($v'' = 1$)]/[IO ($v'' = 0$)] (panel (a)) and [IO ($v'' = 2$)]/[IO ($v'' = 0$)] (panel (b)) for experiments carried out at different low pressures. Nonequilibrium populations can be observed in the initial time steps, suggesting a source of vibrationally excited IO species related to the photolysis flash. Relaxation to thermal equilibrium ratios [IO ($v'' = 1$)]/[IO ($v'' = 0$)] ~0.05 and [IO ($v'' = 2$)]/[IO $v'' = 0$)]) ~0.001 occurs after about 3 ms.

Therefore, the reaction IO + OIO has been finally included in the group of reactions (8).

The observed temporal behaviors are successfully reproduced by neglecting thermal dissociation. This suggests that the IO and OIO dimers could be stable at least on the time scale of our experiments (<30 ms). However, the forward and backward reactions could be encompassed in single effective forward reactions, as a result of undefined minima of the χ^2 function. This possibility is further discussed below.

Finally, the potentially slow dissociation of the IO dimer suggests its attachment to other species. Therefore, the following set of reactions has been included in the mechanism:[51]

$$(IO)_n + IO \rightarrow (IO)_{n+1} \quad n = 1, 2... \tag{11}$$

This, together with

$$(IO)_n + OIO \rightarrow (IO)_nOIO \quad n = 1, 2... \tag{12}$$

leads to a copolymerization mechanism. The rate coefficients of (11) have been assumed to be equal to those of reactions (8) and (9) (k_{IO+R}), and the rate coefficients of (12) are equal to the rates of reactions (7) and (10) (k_{OIO+R}).

Results Obtained with the Proposed Mechanism. The validity of the chemically plausible mechanism, listed in Table 3, has been tested by fitting the simulated concentration versus time curves to the data available (38 datasets). The parameters fit in this manner are the rate coefficients of the channels of the IO self-reaction, the common rate coefficient for reactions (7), (10), and (12), and the common rate coefficient for reactions (8), (9), and (11) (6 free parameters in total). Examples of the results at 40 hPa are shown in Figure 2. The fits show excellent agreement between the simulated and the observed temporal behaviors of I_2, I, IO, and OIO curves within the experimental uncertainties. As no dependence on the buffer gas, $[O_3]_0$ or $[I_2]_0$, can be discerned, the results of all sets of experiments for each pressure have been averaged. The pressure dependence of the rate coefficients obtained is shown in Figures 6 and 10.

The overall rate coefficient of reaction (2) for each pressure can be calculated by adding the rate coefficient of each channel obtained from the optimized simulations (Figure 6). No pressure dependence of the k_2 values obtained in this manner can be discerned outside the error intervals. The weighted average of these values is $k_2 = (7.5 \pm 1.0) \times 10^{-11}$ cm^3 molecule^{-1} s^{-1}, which is in good agreement with the value of k_2 obtained by steady state analysis reported in the previous section. The agreement of the values obtained by simple kinetic analysis and optimized complex simulation can be explained by the small influence of reactions (8), (9), and (11) at the time where IO reaches its maximum. In a sensitivity study, unconstrained simulations of the $I_2/h\nu/O_3$ system with and without these reactions, and subsequent analysis of the calculated [IO] curves with the steady state approach, have shown an effect of these reactions on the k_2 value obtained by this method of less than 6%. The weighted average of the values obtained by both approaches is $k_2 = (7.6 \pm 1.1) \times 10^{-11}$ cm^3 molecule^{-1} s^{-1}.

The rate coefficients of the channels of reaction (2) obtained from the optimized simulations are in agreement with those obtained from simple kinetic analysis (Figure 6). The preferred values are those obtained from optimized simulations, because they are consistent with the complete data recordings and the channel (2a) is explicitly taken into account. The values of k_{2a} and k_{2b} take very low and practically constant values within the uncertainty region in the whole pressure range. On the other hand, the decrease of k_{2c} and $k_{2b} + 0.5k_{2c}$ is accompanied by an increase in the rate coefficient of k_{2d}. Taking into account that the products I + OIO of channel (2c) are unlikely to result from the excited complex IOOI*, these results indicate that the most likely symmetry of the dimer is IOIO.

Sensitivity Studies. To check that the parameters returned by the fit related to the IO self-reaction are unique, the optimized values have been successively varied by an arbitrary amount and fixed at the modified value in the model. The fitting to the simulated curves has subsequently been run with one less free parameter. According to the systematic behavior of residuals

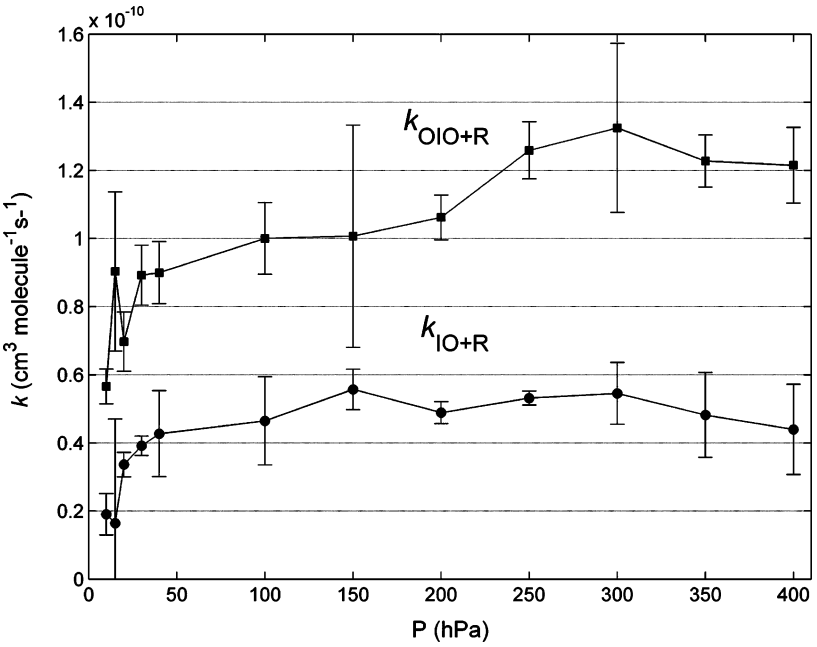

Figure 10. Pressure dependence of the second-order rate coefficients of reactions (8), (9), and (14) (k_{IO+R}) and (7), (10), and (15) (k_{OIO+R}) obtained by complex kinetic simulation (R = any iodine oxide).

and the smaller values of the correlation coefficient, the fits are worse whenever the optimized values are varied by amounts larger than the error intervals shown in Figure 2. The strong interdependence between I, IO, and OIO facilitates the measurability of the changes in the quality of the fit and illustrates how important it is to monitor as many species as possible. In particular, the values of k_2 larger than 9×10^{-11} cm^3 $molecule^{-1}$ s^{-1} lead to a significant underestimation of the simulated [IO] curve. Similarly, values of k_{2b}/k_2 larger than 0.2 lead to an overestimation of the concentration of iodine atoms.

Using the mechanism in Table 3 as reference, we have investigated further possible reactions and their influence on the optimal parameters. In the first place, the role of any O_3 photodissociation has been investigated by using a photolysis frequency, derived from the upper limit of the extent of O_3 photolysis determined experimentally. The inclusion of this process implies a slight correction of the photolysis rate of IO to better fit the initial concentration of IO, thus indicating that both processes are essentially not separable in our data. On the other hand, these processes are irrelevant for the study of the removal of IO and OIO, because $O(^3P)$ is rapidly consumed in an excess of I_2. The only requirement is a good empirical estimation of the initial amount of IO.

An attempt has been made to fit the experimental data with a model containing reversible reactions (7)−(10). The simulated concentrations, the free parameters, and the quality of the fits are sensitive to the values assumed for the reverse rate coefficients of these reactions. A strong dependence of the reverse rate coefficients on cluster size is expected,[26,52] and in fact all attempts to fit the observed data with "global" reverse rate coefficients $k_{ROIO\rightarrow R+OIO}$ and $k_{RIO\rightarrow R+IO}$ failed. The optimized aerosol model parameters of Burkholder et al.[26] indicate that the clusters containing three or more monomer molecules would be stable on the time scale of our experiments. In our sensitivity studies, the dissociation of I_2O_2, I_2O_3, and I_2O_4 have therefore been considered explicitly as:

$$I_2O_2 + M \rightarrow I + OIO + M \quad (13)$$

$$I_2O_3 + M \rightarrow IO + OIO + M \quad (14)$$

$$I_2O_4 + M \rightarrow OIO + OIO + M \quad (15)$$

The inclusion of rapid dissociation of IOIO[11,15] in the chemical mechanism results in a significant regeneration of I and OIO. As a consequence, a different multidimensional χ^2 surface is obtained. In particular, local minima of the new χ^2 are found at different points of the 6-dimensional parameter space. The fitting algorithm searches for these points, i.e., varies some of the free parameters to find the new minima. This is illustrated in Figure 11, where the results of a series of optimized simulations for different values of k_{13}', k_{14}', and k_{15}' are plotted along with the corresponding values of χ^2. In first place, the branching of the IO self-reaction is fixed to the values obtained in the present study by simple kinetic modeling and only k_{IO+R} and k_{OIO+R} are allowed to vary (Figure 11a, red curves). The resulting χ^2 surface is flat for $k_{13}' \leq 100$ s^{-1}, while beyond 100 s^{-1} an increase of χ^2 is observed (thick red line, k_{14}' and k_{15}' are fixed). Therefore, a well-defined lower limit for the lifetime of IOIO is found. On the other hand, if k_{2c} and k_{2d} are allowed to vary, the optimization algorithm finds a prolongation of the flat landscape (Figure 11a, thick black line) for dissociation rates up to 3000 s^{-1} (0.3 ms lifetime) by increasing k_{2c} and decreasing k_{2d} (k_{2a} and k_{2b} do not change significantly). This is a consequence of the relatively weak constraint imposed by the OIO observed curves, whose weight is determined by the ∼23% uncertainty of the absorption cross section. In terms of reproduction of the shape of the OIO curve, these fits are significantly poorer than those obtained for $k_{13}' \leq 100$ s^{-1} (Figure 12c), while the other observed species are similarly well reproduced (Figure 12a,b). The weighting function does not take into account the high accuracy of the optical density curve (i.e., the shape of the concentration curve), whose uncertainty is about 5%. Therefore, we consider that the most consistent set of

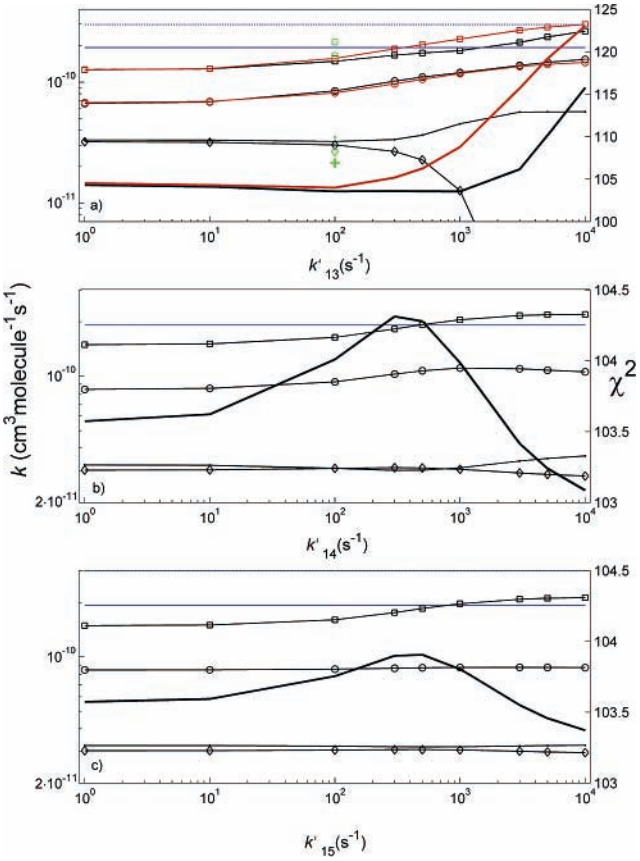

Figure 11. Optimal values of rate coefficients (left axis, thin lines with symbols) and χ^2 values (right axis, thick lines) for different values of the dissociation rate coefficients k_{13}' (panel a), k_{14}' (panel b), and k_{15}' (panel c). Each panel corresponds to the variation of one dissociation coefficient, while the other two were fixed at 100 s^{-1}. Red lines and symbols correspond to fits where k_{2c} (diamonds), k_{2d} (points), k_{IO+R} (circles), and k_{OIO+R} (squares) were allowed to vary. Black lines and symbols: only k_{IO+R} and k_{OIO+R} were allowed to vary. Green symbols: reactions (14) and (15) were not considered. The blue lines indicate the collision frequency factors[49] for OIO calculated assuming a density for I_2O_4 of 2.57 g·cm^{-3} (dashed line)[53] and 4.97 g/cm^{-3} (solid line).[54] The experimental data used in the fits was recorded at 400 hPa (see Figure 12).

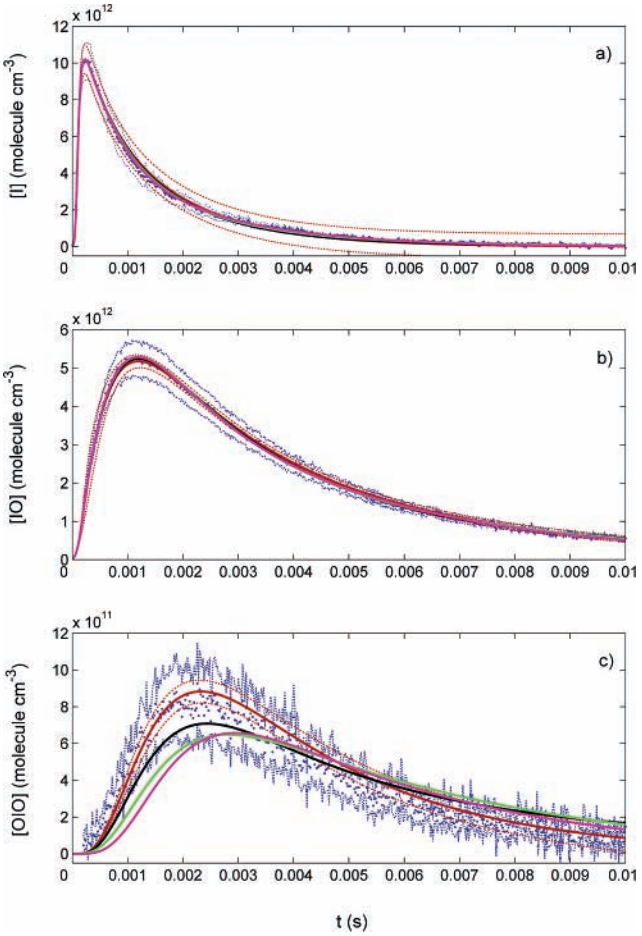

Figure 12. Experimental data (blue points) and optimized fits for 400 hPa. Blue dashed lines indicate the uncertainty of the experimental data. Red lines are concentrations obtained with the proposed model (Table 3) using the optimal values shown in Figure 6. Red dashed lines indicate the estimated uncertainty of the optimized simulation, extrapolated from local first-order sensitivity coefficients.[52] Black, green, and magenta lines correspond to optimized fits for $k_{13}' = 100$ s^{-1}, 500 s^{-1}, and 1000 s^{-1}, respectively.

parameters is that obtained for $k_{13}' \leq 100$ s^{-1}, and as a consequence we suggest a lower limit for the lifetime of I_2O_2 of about 10 ms.

By contrast, the values of k_{2c} and k_{2d} and χ^2 are relatively insensitive to variations in k_{14}' and k_{15}' (Figure 11b,c). The increase of the dissociation rate coefficients is mainly compensated by an increase of the forward rate constant k_{OIO+R} and to a minor extent of k_{IO+R}. Increasing values of k_{14}' and k_{15}' are compensated by values of k_{OIO+R} closer to the collision frequency factor for OIO + OIO (blue lines in Figure 11). A small increase of χ^2 is observed for dissociation rate coefficients larger than 10 s^{-1}, but χ^2 falls again for k_{14}' and $k_{15}' > 1000$ s^{-1}. Divergence of k_{2c} and k_{2d} starts to be important for $k_{14}' > 1000$ s^{-1}, suggesting a lower limit for the lifetime of I_2O_3 of about 1 ms. In summary, the evidence indicating a slow dissociation of I_2O_3 and I_2O_4 is much weaker than in the case of I_2O_2. As a consequence, it can be concluded that the values of k_{OIO+R} and k_{IO+R} obtained with the proposed mechanism (Table 3) are lower limits. Nevertheless, Figure 11 shows that upper limits for both rate coefficients also can be estimated by performing optimized simulations combining $k_{13}' = 100$ s^{-1}, $k_{14}' = 1000$ s^{-1}, and $k_{15}' = 10000$ s^{-1}. These calculations yielded $k_{OIO+R} < (2.9 \pm 0.3) \times 10^{-10}$ cm^3 $molecule^{-1}$ s^{-1} and $k_{IO+R} < (1.0 \pm 0.2) \times 10^{-10}$ cm^3 $molecule^{-1}$ s^{-1} at 400 hPa. The introduction in the mechanism of a 10-fold slower dissociation for the oligomers containing 3 monomer molecules did not change these upper limits significantly.

Reactions (11) and (12) have been included in the mechanism as a logical consequence of the potentially longer lifetime of the IO dimer. The quality of the fits is slightly improved by including these reactions (see Figure 11a). The common rate coefficient for reactions (7), (10), and (12), (k_{OIO+R}), obtained with the proposed mechanism is 30% smaller than the corresponding result if only reactions (7) and (10) are considered (green symbols in Figure 11a). Similarly, the common rate coefficient for reactions (8), (9), and (11), (k_{IO+R}), is about 40% smaller with respect to the result obtained for reactions (8) and (9) only. The kinetic parameters of reaction (2) change slightly by the inclusion of these reactions.

The reaction of IO with O_3 is very exothermic and could be a potential candidate for the additional sink of IO observed. However, its rate coefficient would have to be of about 5×10^{-14} cm^3 $molecule^{-1}$ s^{-1} to account for this sink completely. The analysis of the χ^2 surface of the optimized simulations is insensitive to this reaction for rate coefficients smaller than 10^{-14} cm^3 $molecule^{-1}$ s^{-1}. These values are significantly larger than the estimations previously reported[26,50] and can be see as rough upper limits. On the other hand, an upper limit for the rate

TABLE 4: Determinations of the IO Self-Reaction Rate Coefficient at 295−298 K

ref	system[a]	$[IO]_0$ (10^{13} molecule cm^{-3})	P (hPa)	method[b]	k_2 (10^{-11} cm^3 molecule^{-1} s^{-1})	k_2/σ_{IO} (10^6 cm s^{-1})
Sander[13]	O_2/I_2	2−20	28−933	k/σ, second order	5.3 ± 0.3	1.8 ± 0.1
Stickel et al.[55]	O_3/I_2; I_2/O_3	not instantaneous	1013	(σ,k), complex	6.6 ± 2.8	
Lazlo et al.[56]	N_2O/I_2	0.2−0.3	80−813	k/σ, second order	8.0 ± 1.7	2.86
Harwood et al.[14]	N_2O/I_2	0.5−2	813	k, second order	9.9 ± 1.5	2.75
Vipond et al.[11]	O_2/CF_3I	∼0.01	2.5−3	k, complex	9.3 ± 1.0	
Atkinson et al.[63]	N_2O/CF_3I	0.1−1.2	12.5; 40	k, complex	10 ± 3	
Ingham et al. [18]	O_3/I_2	<0.5	80	k/σ, second order	9.0 ± 1.7	2.5 ± 0.6
Bloss et al.[31]	N_2O/I_2	2−10	133−1013	k, complex	8.2 ± 1.3	
Atkinson et al.[10]				review	9.9 ± 1.0	2.75
this work	I_2/O_3	not instantaneous	10−400	k, steady state k, complex	7.6 ± 1.1	

[a] The photochemical system is described by the two molecular precursors of IO. The first one indicates the molecule that releases free atoms after microwave discharge, photolysis, or fast reaction. [b]The method is described by the quantities determined (k/σ, k, or σ) and the kinetic approach employed (complex kinetic modeling, second-order fitting of the IO decay, or steady state at the maximum of [IO](t)).

coefficient of the O_3 + OIO reaction of 5×10^{-14} cm^3 molec^{-1} s^{-1} has been estimated.

Discussion

Overall Rate of the IO Self-Reaction. The determination of k_2 in systems with ozone has been avoided in most previous studies. In the presence of ozone, IO presents second-order behavior for low I atom concentrations with an effective rate coefficient $k_{2eff} = k_2(1 - \alpha) < k_2$, which only accounts for non-iodine atom products. This approach was used in two previous studies to determine the iodine atom yield, α, of the IO self-reaction.[13,14] Stickel et al.[55] reported a value of $k_2 = (6.6 \pm 2.0) \times 10^{-11}$ cm^3 molecule^{-1} s^{-1} at 1013 hPa, which is currently thought to be rather a k_{2eff} value. By contrast, we have taken into account the recycling of iodine atoms both in the conventional analysis (equation (ii)) and in the complex modeling (Table 3). The pressure independent value obtained is about 20% lower than the IUPAC recommendation.[10] According to our sensitivity studies, further potential sources of IO, which might be active in the $I_2/h\nu/O_3$ system and not in the $N_2O/h\nu/I_2$ system, cannot explain this difference.

In systems in which the reaction of $O(^3P)$ and I_2 is the only source of IO, second-order decays of IO have been reported with rate coefficients between 8×10^{-11} and 10^{-10} cm^3 molecule^{-1} s^{-1}, independent of P, $[I_2]$, and $[IO]_0$[14,20,31,56] (see Table 4). These are considered the "cleanest" chemical systems for the measurement of k_2. The agreement between the values of k_2/σ_{IO}(427.2 nm) and the consensus about the absorption cross section of IO[14,32,57] are the basis of the IUPAC recommendation: $k_2 = (9.9 \pm 1.0) \times 10^{-11}$ cm^3 molecule^{-1} s^{-1}. However, other problems associated to the $N_2O/h\nu/I_2$ system might affect the determinations of the rate coefficient of reaction (2). For example, Sander[13] obtained a value of $k_2 = (5.3 \pm 0.3) \times 10^{-11}$ cm^3 molecule^{-1} s^{-1} in the $O_2/h\nu/I_2$ system. Deviations of IO from second order for $T < 298$ K were reported by Harwood et al.,[14] who found them to be consistent with the reaction of IO with a product of its self-reaction. In addition, large amounts of free iodine atoms are available for reaction with iodine oxides.[19] A strong argument supporting the determination reported here is the ability to simultaneously reproduce the concentration of three observed species sensitive to this rate coefficient (I, IO, and OIO) rather than only IO.

To investigate the potential influence of the reactions (7)−(12) on the analysis of IO decays measured in the $N_2O/h\nu/I_2$ system, unconstrained simulations of this chemistry at 10 hPa and 1013 hPa with the initial conditions employed by Harwood et al.[14] have been performed. The branching ratios of reaction (2) at 1013 hPa have been taken from Bloss et al.[31] An overall rate coefficient $k_2 = 8 \times 10^{-11}$ cm^3 molecule^{-1} s^{-1} has been considered. Iodine atom reactions reported by Joseph et al.[19] also have been included. Under some circumstances, the simulated IO decays fit to a good approximation to second-order behavior with an enhanced second-order rate coefficient of $\sim 10^{-10}$ cm^3 molecule^{-1} s^{-1}. This 20% enhancement of the second-order rate coefficient results from the inclusion of the set of reactions (8) in these simulations. A pressure dependence of the apparent rate coefficient is not observed because k_{IO+R} is near its high-pressure limit (Figure 10b). On the other hand, these simulations show a dependence of the calculated k_2 on $[IO]_0$, which has not been observed in previous studies.[14,56] In addition, the lack of knowledge about the iodine abstraction reactions[15,49] introduces large uncertainties in these simulations. However, in agreement with Lazlo et al., it might be concluded[56] that the second-order behavior of IO is insufficient in this case to validate a chemical mechanism. A new experimental study of the $N_2O/h\nu/I_2$ system with a multichannel approach as in the present work would contribute to solve these open questions.

Branching of the IO Self-Reaction. Table 5 contains a summary of the IO self-reaction branching data published so far. The branching ratios and yields are also plotted as a function of pressure in Figure 13. The IO self-reaction is bimolecular and in principle can proceed through excited complexes of different symmetries.[11,15] According to ab initio calculations, four I_2O_2 isomers are thermodynamically allowed from IO + IO. The formation of the most stable dimer (IIO_2) from the IO self-reaction would require extensive rearrangement of bonds. The upper limit of 5% for the yield of I_2 reported by Sander,[13] consistent with our results, indicates that collisions on the OIIO* potential energy surface are minor. The intermediates IOOI* and IOIO* would end up in the reaction products 2I + O_2 (channel 2b) and I + OIO (channel 2c) respectively, although they could also be collisionally stabilized (channel 2d).

Our results show that collisions on the IO/OI surface (channel 2b) are minor (∼10%). No pressure dependence of this channel can be distinguished in our data. This indicates that IOOI* cannot be stabilized in this range of pressures. On the other hand, most collisions take place on the IO/IO surface, as expected from the interaction of two strong dipoles. This conclusion is consistent with the tendency of the halogen monoxides to react with each other via an alternating excited complex XOYO*, when proceeding from chlorine via bromine to iodine. The weight of channel (2c) is overtaken by channel (2d) as pressure increases, thus indicating the stabilization of IOIO*. Rapid dissociation of IOIO has been found to be hardly compatible with our observations and with the most recent results of k_2 reported in the literature.

TABLE 5: Determinations of the IO Self-Reaction Branching Ratios at 295−298 K

ref	species monitored	P (hPa)	k_{2a}/k_2	k_{2b}/k_2	k_{2c}/k_2	k_{2d}/k_2	$(k_{2b} + 0.5k_{2c})/k_2$	$(k_{2a} + 0.5k_{2c} + k_{2d})/k_2$
Jenkin et al.[12]	I_2, O_3	1013	0				0.20 ± 0.07[a,b]	0.80 ± 0.07
Sander[13]	IO, I_2	28	<0.05				0.42 ± 0.12	0.58 ± 0.12
		867					0.17 ± 0.12	0.83 ± 0.12
Harwood et al.[14]	IO, I_2	28[c]	<0.30				0.50 ± 0.16	0.51 ± 0.1
		867					0.12 ± 0.16	0.78 ± 0.16
Vipond et al.[11]	IO, I	2.5−3		>0.52 ± 0.2	<0.44±0.2		0.78 ± 0.10	0.22±0.10
Bloss et al.[31]	IO, I_2, OIO	>800	<0.05	0.11 ± 0.04	0.38 ± 0.08	0.46 ± 0.06	0.3	>0.65
Joseph et al.[19]	OIO	53		>0.68	0.31 ± 0.10		>0.83	<0.17
this work	IO, I_2, I, OIO	10	~0.05	0.09 ± 0.06	$0.74 \pm .10$	0.14 ± 0.08	0.44 ± 0.11	0.52 ± 0.11
		400			0.45 ± 0.10	0.44 ± 0.13	0.28 ± 0.14	0.72 ± 0.14

[a] The branching ratios directly deduced from experimentally determined quantities are indicated in bold case. [b]Jenkin et al.[12] obtained the ratio of the rate coefficient of the iodine producing channels to that of the noniodine producing channels (0.25 ± 0.11). At that time, no evidence for channel (2c) had been found,[46] and therefore the authors postulated that $k_{2b}/k_{2d} = 0.25$. The updated ratio must include the contribution of one-half of (2c). We have derived the iodine atom yield directly from the ratio reported in this reference.[12] [c]We have deduced that the pressure range of the values reported refers to the same considered by Sander.[13]

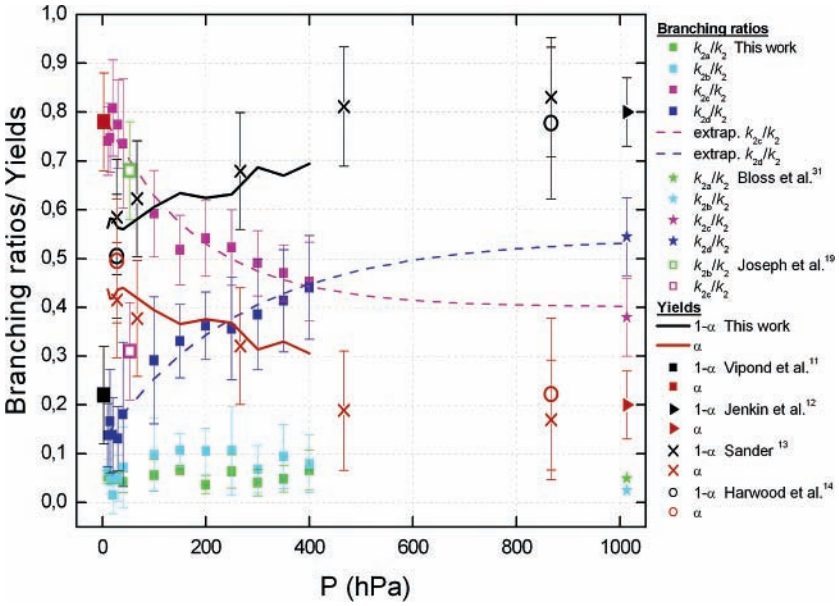

Figure 13. Literature values of branching ratios and yields. Branching ratios as a function of pressure are given by scatter plots of colored symbols (k_{2a}/k_2, green; k_{2b}/k_2, cyan; k_{2c}/k_2, magenta; k_{2d}/k_2, blue). The iodine atom yields (α) are represented by red symbols. The 1 - α values are represented by black symbols. Extrapolations to tropospheric conditions of the results obtained in the present study for k_{2c}/k_2 and k_{2d}/k_2 are indicated by dashed lines.

In the calculations reported by Misra and Marshall,[15] it was assumed that the contributions of channels (2a) and (2b) were small. They suggested that a pressure independent channel (2c) would dominate over (2d), which is consistent with the pressure independence of the overall rate coefficient. The results reported by Vipond et al.[11] ($k_{2c}/k_2 = 0.44 \pm 0.20$ at 1.9−2.2 Torr), Joseph et al.[19] ($k_{2c}/k_2 = 0.31 \pm 0.10$ at 40 Torr), and Bloss et al.[31] ($k_{2c}/k_2 = 0.38 \pm 0.08$ at 760 Torr) seem to be consistent with a pressure independent branching ratio for channel (2c). However, these three studies disagree with Misra and Marshall about the importance of channels (2b) and (2d). On the other hand, the pressure dependence of $(1 - \alpha)$ observed by Sander,[13] Harwood et al.,[14] and our experimental results are inconsistent with a pressure independent branching. Saunders and Plane[28] have suggested that the I−OIO bond strength determined ab initio[15,28] could be underestimated by about 20 kJ mol^{-1}, thus explaining the divergence between theoretical predictions and experimental results.

The directly measured quantity reported by Bloss et al.[31] (k_{2c}) is consistent with the extrapolation of our determination for channel (2c) toward atmospheric pressure (Figure 13) by using an empirical exponential decay of the form $f(P) = A + Be^{-cP}$ (where A, B and C are constants). From the work of Jenkin et al.,[12] an iodine atom yield $\alpha = 0.2$ can be deduced. By combining this with the result of Bloss et al., a value of $k_{2d}/k_2 \sim 0.5$ under tropospheric conditions can be estimated. This value also is consistent with the extrapolation of our determination by using an exponential growth of the form $f(P) = A - Be^{-cP}$.

Vipond et al.[11] reported a yield of iodine atoms from the self-reaction of $\alpha = 0.78 \pm 0.10$ at 1.9−2.2 Torr (2.5−3 hPa), roughly 2 times larger than our value at 10 hPa. As the pressure in this case would be too low to enable the stabilization of the IO dimer, this value implies that other iodine producing channels apart from (2c) must be active. The chemical system $O_2/h\nu/CF_3I$ in a discharge flow tube setup is extremely complex due to the interaction of NO and CF_3 with IO and to wall losses. Vipond et al. addressed these issues in detail by determining the required rate coefficients and considering the corresponding reactions in a numerical model. This is critical to avoid the overestimation of the amount of IO consumed and of I produced via reaction (2). Although there is no clear reason for the discrepancy, unaccounted losses of the iodine atoms produced by the reaction of IO and NO in the interval between injection of NO and detection of I by resonance fluorescence (4 ms) would lead to an underestimation of the amount of IO and to a subsequent overestimation of α.

Joseph et al.[19] reported a branching ratio for channel (2c) at 40 Torr (52 hPa) of $k_{2c}/k_2 = 0.31 \pm 0.10$ and, assuming that channels (2a) and (2d) are not active, they derived $k_{2b}/k_2 = 0.68$. By accounting for the difference in the absorption cross sections employed to scale the OIO transient absorption ($\sim$ 15% larger than our determination[19,32]) and the overall rate coefficient (Joseph et al.[19] use the value of Bloss et al.[31]), a value of $k_{2c}/k_2 \sim 0.45$ is obtained ($k_{2b}/k_2 = 0.55$), still far from the value of about 0.7 that we have obtained at 40 hPa. This disagreement might be the result of a small overestimation of the excimer laser fluence, leading to an overestimation of the initial amount of IO produced from the photolysis of N_2O. This would cause a significant underestimation of k_{2c}/k_2, because in steady state of OIO this ratio depends on $[IO]^{-2}$.

Fates of OIO and IOIO and Link to the Higher Oxides. To date only one study of the complex kinetic behavior of OIO has been published. Joseph et al.[19] concluded that in the absence of O_3, the I + OIO reaction is responsible for the disappearance of OIO. Our work constitutes the first investigation of the OIO temporal behavior reported in the literature at a variety of conditions in the presence of ozone. Burkholder et al.[26] succeeded in reproducing the particle production in a Teflon bag experiment by assuming OIO homogeneous nucleation and using parametrized thermodynamics to model the backward rate coefficients. They used forward coefficients derived from kinetic theory[52] ($\geq 3 \times 10^{-10}$ cm^3 molecule^{-1} s^{-1}) and did not consider participation of IO in the cluster formation. Our study has shown that attachment of IO to other species, and in particular the reaction IO + OIO $\rightarrow$ I_2O_3 (8, $n = 1$), must be included in the mechanism to reproduce the observed IO and OIO concentrations and to obtain reasonable values for k_{OIO+R} ($n < 4$), which otherwise would be larger than 5×10^{-10} cm^3 molecule^{-1} s^{-1}. A recent modeling study by Pirjola et al.[27] shows good correlation between observed and modeled particle size distributions in chamber experiments[58] by including reaction (8, $n = 1$) and considering I_2O_3 in the first cluster size section. However, their model apparently does not consist of a binary nucleation or copolymerization of IO and OIO. The good performance of our model in reproducing the experimental data also depends on the polymerization of IO units.

As a consequence of the introduction of reactions (8), (9), and (11) in the chemical model, the optimal values of k_{OIO+R} are smaller than 3×10^{-10} cm^3 molecule^{-1} s^{-1} (see Figure 11, panels b and c). The optimal values obtained for k_{IO+R} are a factor of 2 or 3 smaller than those obtained for k_{OIO+R}. On the other hand, the IO and OIO collision frequency factors are very similar. This could indicate that the kinetic theory does not account for the rate coefficients of forward reactions in the first steps of the nucleation process. The assumption of spherical geometry is probably inadequate for polymeric structures in which steric constraints might play a role. However, the ability to reproduce the sinks of IO and OIO with only two rate coefficients for all reactions encompassed in (7)−(12) might result from the fact that IO + OIO (8, $n = 1$) and OIO + OIO (7, $n = 1$) are rate determining. The rate coefficients obtained in particular for these two reactions are smaller than the capture rate coefficients from the dipole−dipole interaction.[19,28] This also suggests the existence of steric constraints, although the possibility of different short dissociation lifetimes of the polymeric adducts cannot be discarded.

From the results of the continuous, I_2-photosensitized ozone destruction experiments carried out by Jenkin et al.,[12] an iodine atom yield $\alpha = 0.2$ from reaction (2) can be deduced by assuming that the only fate of I and O_3 is reaction (1). This suggests that the lifetime of the IO dimer could be even longer than the lower limit of 10 ms reported here. The participation of this species in gas to particle conversion has been hypothesized in a number of previous publications.[27,57] In laboratory studies, this depends most likely on the amount of radicals generated. Reactions (11) and (12) might be significant with respect to thermal decomposition at very high concentrations of IO and OIO.

The mechanism proposed (Table 3) indicates that higher iodine oxides will form with the stoichiometric ratio O/I $\leq$ 2. However, in a previous study performed in our laboratory, a white solid deposit was collected and identified as I_2O_5.[60] Saunders and Plane[28] have also collected particles with I_2O_5 stoichiometry. In the present study, performed with significantly different mixing ratios of precursors, a pale yellow powder similar to that reported by Cox and Coker[29] has been observed. This suggests that the stoichiometry of the solid products might depend on the concentration of precursors employed. Assuming that successive reaction of iodine oxides with ozone leads to I_2O_5,[28] the amount of iodine and ozone employed might determine if these oxidation steps, or rather polymerization, dominate the production of higher iodine oxides. However, the short lifetime predicted for I_2O_4,[26,28] which is compatible with our results, would slow down dramatically the formation of I_2O_5.

To date, there are no laboratory studies reporting simultaneous measurements of gas-phase iodine oxides, polymers, and particle production. Further investigations are required to achieve a spectroscopic assignment of the higher order oxides. Kinetic studies of the thermal decomposition of I_2O_2, I_2O_3, and I_2O_4 and of the polymerization mechanism would require the implementation of methods capable of simultaneous time-resolved monitoring of the gas phase and the nascent polymers.

Atmospheric Relevance. Under atmospheric conditions, the iodine atom yield of reaction (2) is small. The ozone destroying potential of the iodine chemistry depends on the fate of the molecular products of channels (2c) and (2d). Recent studies[19,20] indicate that OIO is relatively photostable, so that a small additional yield of iodine atoms is obtained from its photolysis. According to our results, IOIO seems to be thermally stable at least on a time scale of tens of milliseconds. If the lifetime is actually less than 1 s, the main atmospheric fate of IOIO would be dissociation, because the atmospheric mixing ratios of potential reaction partners (e.g., IO, OIO, O_3) are not large enough. As a result, the effective iodine atom yield of the IO self-reaction would be enhanced to up to 60%, as assumed in previous publications.[26,61] This would imply a larger ozone-destroying potential of the iodine chemistry.[33] On the other hand, the result of Jenkin et al.[12] seems to indicate a longer lifetime. The main consequence of this (assuming slow photolysis of I_2O_2) would be the partitioning of a larger fraction of iodine to aerosol by nucleation processes or by heterogeneous uptake.

The effective yield of OIO from reaction (2) varies between 20% and 40% depending on the stability of IOIO. The reaction of IO + OIO seems to be rapid enough to explain the disappearance of OIO from the MBL during the day.[3,61,62] If I_2O_4 is as short-lived as indicated by quantum calculations,[28] this species represents a "bottle neck" for the two gas to particle conversion models proposed (OIO polymerization and O_3 oxidation steps). The reaction IO + OIO, forming the thermally stable species I_2O_3,[28] and the participation of IO in a copolymerization mechanism could bring into better agreement the IO and OIO steady state mixing ratios with the particle concentration and nucleation rates observed in the MBL.

Conclusions

The overall rate coefficient of the IO self-reaction at 298 K has been found to be pressure independent in the range of pressures between 10 and 400 hPa of N_2 and O_2. By contrast, the branching of this reaction has been found to be pressure dependent. The yield of iodine atoms and of OIO decreases as the pressure increases. Under tropospheric conditions, the main product of this reaction is the IO dimer. According to the pressure dependence exhibited by the different channels of the IO self-reaction, it can be concluded that the most plausible geometry of the IO dimer is IOIO. The lifetime of IOIO seems to be significantly larger than predicted by theoretical calculations.

The result obtained for the rate coefficient of the IO self-reaction is about 20% lower than the IUPAC recommendation. This fact is consistent with a fast reaction of IO and OIO. Its rate coefficient is pressure independent for $P > 40$ hPa. Evidence for the "self-reaction" of OIO and for the attachment of IO and OIO to higher iodine oxides also has been found

Acknowledgment. The authors thank Dr. Andrés Hernández and Professor Dr. Plane for helpful comments and suggestions. This work was partially founded by the German Space Agency (Contract 50EP9207 'SCIAMACHY' and project LVA 01/003), the European Union (Contract EVK2-CT2001-00104 "THALOZ"), the EU-ACCENT Network of Excellence, and the University and the State of Bremen.

References and Notes

(1) Miyake, Y.; Tsungoai, S. *J. Geophys. Res.* **1963**, *68*, 3989−3994.
(2) Garland, J. A.; Curtis, H. *J. Geophys. Res.* **1981**, *86* (C4), 3183−3196.
(3) Saiz-López, A.; Plane, J. M. C. *Geophys. Res. Lett.* **2004**, *31*, L04112.
(4) McFiggans, G.; Coe, H.; Burgess, R.; Allan, J.; Cubison, M.; Alfarra, M. R.; Saunders, R.; Saiz-Lopez, A.; Plane, J. M. C.; Wevill, D.; Carpenter, L. J.; Rickard, A. R.; Monks, P. S. *Atmos. Chem. Phys.* **2004**, *4*, 701−713.
(5) Lovelock, J. E.; Maggs, K. J.; Wade, R. J. *Nature* **1973**, *241*, 194−196.
(6) Carpenter, L. J.; Sturges, W. T.; Penkett, S. A.; Liss, P. S.; Alicke, B.; Hebestreit, K.; Platt, U. *J. Geophys. Res.* **1999**, *104*(D1), 1679−1689.
(7) Alicke, B.; Hebestreit, K.; Stutz, J.; Platt, U. *Nature* **1999**, *397*, 572−573.
(8) Allan, B. J.; McFiggans, G.; Plane, J. M. C.; Coe, H. *J. Geophys. Res.* **2000**, *105*, 14363−14370.
(9) Chameides, W. L.; Davis, D. D. *J. Geophys. Res.* **1980**, *85*, 7383−7398.
(10) Atkinson, R.; Baulch, D. L.; Cox, R. A.; Crowley, J. N.; Hampson, R. F.; Hynes, R. G.; Jenkin, M. E.; Rossi, M. J.; Troe, J. *Atm. Chem. Phys. Disc.* 2006, *6*, 2281−2702.
(11) Vipond, A., Canosa-Mas, C. E.; Flugge, M. L.; Gray, D. J.; Shallcross, D. E.; Shaha, D.; Wayne, R. P. *Phys. Chem. Chem. Phys.* **2002**, *4*, 3648−3658.
(12) Jenkin, M. E.; Cox, R. A.; Candeland, D. E. *J. Atmos. Chem.* **1985**, *2*, 359−375.
(13) Sander, S. P. *J. Phys. Chem.* **1986**, *90*, 2194−2199.
(14) Harwood, M. H.; Burkholder, J. B.; Hunter, M.; Fox, R. W.; Ravishankara, A. R. *J. Phys. Chem. A* **1997**, *101*, 853−863.
(15) Misra, A.; Marshall, P. *J. Phys. Chem.* **1998**, *102*, 9056−9060.
(16) Allan, B. J.; Plane, J. M. C.; McFiggans, G. *Geophys. Res. Lett.* **2001**, *28*, 1945−1948.
(17) Peters, C.; Pechtl, S.; Stutz, J.; Hebestreit, K.; Hönninger, G.; Heumann, K. G.; Schwarz, A.; Winterlik, J.; Platt, U. *Atmos. Chem. Phys.* **2005**, *5*, 3357−3375.
(18) Ingham, T.; Cameron, M.; Crowley, J. N. *J. Phys. Chem. A* **2000**, *104*, 8001−8010.
(19) Joseph, D. M.; Ashworth, S. H.; Plane, J. M. C. *J. Photochem. Photobiol., A* **2005**, *176*, 68−77.
(20) Tucceri, M. E.; Hölscher, D.; Rodriguez, A.; Dillon, T. J.; Crowley, J. N. *Phys. Chem. Chem. Phys.* **2006**, *8*, 834−846.
(21) Plane, J. M. C.; Joseph, D. M.; Allan, B. J.; Ashworth S. H.; Francisco, J. S. *J. Phys. Chem A* **2006**, *110(1)*, 93−100.
(22) Cox, R. A.; Bloss, W. J.; Jones, R. L.; Rowley, D. M. *Geophys. Res. Lett*. **1999**, *26*(13) 1857−1860.
(23) O'Dowd, C. D.; Jimenez, J. L.; Bahreini, R.; Flagan, R. C.; Seinfeld, J. H.; Kulmala, M; Pirjola, L.; Hoffmann, T. *Nature* **2002**, *417*, 632−636.
(24) Hoffmann, T.; O'Dowd, C. D.; Seinfeld, J. H. *Geophys. Res. Lett.* **2001**, *28*, 1949−1952.
(25) Jimenez, J. L.; Bahreini, R.; Cocker III, D. R.; Zhuang, H.; Varutbangkul, V.; Flagan, R. C.; Seinfeld, J. H.; O'Dowd, C. D.; Hoffmann, T. *J. Geophys. Res.* **2003**, *108* (D10), 4318.
(26) Burkholder, J. B.; Curtius, J.; Ravishankara, A. R.; Lovejoy, E. R. *Atmos. Chem. Phys.* **2004**, *4*, 19−34.
(27) Pirjola, L.; O'Dowd, C. D.; Yoon, Y. J.; Sellegri, K. *Environ. Chem.* **2005**, *2*, 271−281.
(28) Saunders, R. W.; Plane, J. M. C. *Environ. Chem.* **2005**, *2*, 299−303.
(29) Cox, R. A.; Coker, G. B. *J. Phys. Chem.* **1983**, *87*, 4478−4484.
(30) Jenkin, M. E.; Cox, R. A. *J. Phys. Chem.* **1985**, *89*, 192−199.
(31) Bloss, W. J.; Rowley, D. M.; Cox, R. A.; Jones, R. L. *J. Phys. Chem. A* **2001**, *105*, 7840−7854.
(32) Gómez, Martín, J. C.; Spietz, P.; Burrows, J. P. *J. Photochem. Photobiol., A* **2005**, *176*, 15−38.
(33) McFiggans, G.; Plane, J. M. C.; Allan, B. J.; Carpenter, L. J.; Coe, H.; O'Dowd, C. D. *J. Geophys. Res.* **2000**, *105* (D11), 14371−14385.
(34) Rabinowitch, E.; Wood, W. *J. Chem. Phys.* **1936**, *4*, 358−362.
(35) Brewer, L.; Tellinghuisen, J. *J. Chem. Phys.* **1972**, *56*, 3929−3938.
(36) Young, A. T.; Houston, P. L. *J. Chem. Phys.* **1983**, *78*, 2317−2326.
(37) Matsumi, Y.; Comes, F. J.; Hancock, G.; Hofzumahaus, A.; Hynes, A. J.; Kawasaki, M.; Ravishankara, A. R. *J. Geophys. Res.* **2002**, *107* (D3), 4024−4035.
(38) Gómez Martín, J. C.; Spietz, P.; Orphal, J; Burrows, J. P. *Spectrochim. Acta, Part A* **2004**, *60*, 2673−2693.
(39) Spietz, P.; Gómez, Martín, J. C.; Burrows, J. P. *Spectrochim. Acta, Part A* **2006**, *64*, 722−735.
(40) Spietz, P.; Gómez Martín, J. C.; Burrows, J. P. *Atmos. Chem. Phys.* **2006**, *6*, 2177−2191.
(41) Spietz, P.; Gross, U.; Smalins, E.; Orphal, J.; Burrows, J. P. *Spectrochim. Acta, Part B* **2001**, *56*, 2465−2478.
(42) Shampine, L. F.; Reichelt, M. W. *SIAM J. Sci. Comput.* **1997**, *18*, 1−22.
(43) Rowley, D. M.; Harwood, M. H.: Freshwater, R. A.; Jones, R. L. *J. Phys. Chem* **1996**, *100*, 3020−3029.
(44) MATLAB version 6.5, Release 14 with Service Pack 3; The MathWorks Inc.: Natick, MA, 2002.
(45) Press, W. H.; Teukolsky, S. A.; Vetterling, W. T.; Flannery, B. P. *Numerical Recipes in C. The Art of Scientific Computing*, 2nd edition; Cambridge University Press: Cambridge, U.K., 1992; pp. 666−668.
(46) Himmelmann, S.; Orphal, J.; Bovensmann, H.; Richter, A.; Ladstaetter-Weissenmayer, A.; Burrows, J. P. *Chem. Phys. Lett.* **1996**, *251*, 330−334.
(47) Spietz, P.; Gómez Martín, J. C.; Burrows, J. P. *J. Photochem. Photobiol., A* **2005**, *176*, 50−67.
(48) Bekooy, J. B.; Leo, Meerts, W.; Dymanus, A. *J. Mol. Spec.* **1983**, *102*, 320−343.
(49) Laidler, K. J. *Chemical Kinetics*, 3rd edition; Harper Collins Publishers: New York, 1987; pp. 277−340.
(50) Larin, I. K.; Nevozhai, D. V.; Spasskii, A. I.; Trofimova, E. M.; Turkin, L. E. *Kinet. Catal.* **1999**, *40*, 487−495.
(51) Chatfield, R. B.; Crutzen, P. J. *J. Geophy. Res.* **1990**, *95D*, 22319−22341.
(52) Seinfeld, J. H.; Pandis, S. N. *Atmospheric Chemistry and Physics*; John Wiley & Sons, New York, 1998; pp. 222−225.
(53) Fjellvåg, H.; Kjekshus, A. *Acta Chem. Scand.* **1994**, *48*, 815−822.
(54) Daehlie, G.; Kjekshus, A. *Acta Chem. Scand.* **1964**, *18*, 144−156.
(55) Stickel, R. E.; Hynes, A. J.; Bradshaw, J. D.; Chameides, W. L.; Davies, D. D. *J. Phys. Chem.* **1988**, *92*, 1862−1864.
(56) Lazlo, B.; Kurylo, M. J.; Huie, R. E. *J. Phys. Chem.* **1995**, *99*, 11701−11707.
(57) Dillon, T.J.; Tucceri, M.E.; Hölscher, D.; Crowley, J.N. *J. Photochem. Photobiol., A*, **2005**, *176*, 3−14.
(58) Sellegri, K.; Yoon, Y. J.; Jennings, S. G.; O'Dowd, C. D.; Pirjola, L.; Cautenet, S.; Chen, H.; Hoffmann, T. *Environ. Chem.* **2005**, *2*, 260−270.
(59) Saiz-Lopez, A.; Plane, J. M. C.; McFiggans, G.; Williams, P. I.; Ball, S. M.; Bitter, S. M.; Jones, R. L.; Hongwei, C.; Hoffmann, T. *Atm. Chem. Phys.* **2006**, *6*, 883−895.
(60) Himmelmann, S. Ph.D. Thesis, University of Bremen, Institute of Environmental Physics, Bremen, Germany, 1997.
(61) Pechtl, S.; Lovejoy, E. R.; Burkholder, J. B.; von Glasow, R. *Atm. Chem. Phys.* **2006**, *6*, 505−523.
(62) Saiz-Lopez, A.; Shillito, J. A.; Coe, H.; Plane, J. M. C. *Atm. Chem. Phys.* **2006**, *6*, 1513−1528.
(63) Atkinson, D. B.; Hudgens, J. W.; Orr-Ewing, A. J. *J. Phys. Chem.* **1999**, *103*, 6173−6180.
(64) DeMore, W. B.; Sander, S. P.; Goldan, D. M.; Hampson, R. F.; Kurylo, M. J.; Howard, C. J.; Ravishankara, A. R.; Kolb, C. E.; Molina, M. J. *Chemical Kinetics and Photochemical Data for use in Stratospheric Modeling: Evaluation 14*; Jet Propulsion Laboratory: Pasadena, CA, 2003.